# Example-Based Sampling with Diffusion Models

Bastien Doignies, Nicolas Bonneel, David Coeurjolly, Julie Digne, Lois Paulin, Jean-Claude Iehl, Victor Ostromoukhov

# Example-Based Sampling with Diffusion Models

Bastien Doignies
Univ Lyon, UCBL, CNRS, INSA Lyon
France
bastien.doignies@liris.cnrs.fr

Nicolas Bonneel
Univ Lyon, CNRS, UCBL, INSA Lyon
France
nicolas.bonneel@liris.cnrs.fr

David Coeurjolly
Univ Lyon, CNRS, UCBL, INSA Lyon
France
david.coeurjolly@liris.cnrs.fr

Julie Digne
Univ Lyon, CNRS, UCBL, INSA Lyon
France
julie.digne@liris.cnrs.fr

Lois Paulin
Univ Lyon, UCBL, CNRS, INSA Lyon, Adobe
France
paulin@adobe.com

Jean-Claude Iehl
Univ Lyon, UCBL, CNRS, INSA Lyon
France
jean-claude.iehl@liris.cnrs.fr

Victor Ostromoukhov
Univ Lyon, UCBL, CNRS, INSA Lyon
France
victor.ostromoukhov@liris.cnrs.fr

## ABSTRACT

Much effort has been put into developing samplers with specific properties, such as producing blue noise, low-discrepancy, lattice or Poisson disk samples. These samplers can be slow if they rely on optimization processes, may rely on a wide range of numerical methods, are not always differentiable. The success of recent diffusion models for image generation suggests that these models could be appropriate for learning how to generate point sets from examples. However, their convolutional nature makes these methods impractical for dealing with scattered data such as point sets. We propose a generic way to produce 2-d point sets imitating existing samplers from observed point sets using a diffusion model. We address the problem of convolutional layers by leveraging neighborhood information from an optimal transport matching to a uniform grid, that allows us to benefit from fast convolutions on grids, and to support the example-based learning of non-uniform sampling patterns. We demonstrate how the differentiability of our approach can be used to optimize point sets to enforce properties.

## CCS CONCEPTS

• **Computing methodologies** → **Neural networks**; **Computer graphics**.

## KEYWORDS

diffusion models, sampling, point patterns, example-based synthesis

**ACM Reference Format:**
Bastien Doignies, Nicolas Bonneel, David Coeurjolly, Julie Digne, Lois Paulin, Jean-Claude Iehl, and Victor Ostromoukhov. 2023. Example-Based Sampling with Diffusion Models. In *SIGGRAPH Asia 2023 Conference Papers (SA Conference Papers '23), December 12–15, 2023, Sydney, NSW, Australia.* ACM, New York, NY, USA, 11 pages. https://doi.org/10.1145/3610548.3618243

*SA Conference Papers '23, December 12–15, 2023, Sydney, NSW, Australia*


## 1 INTRODUCTION

A wide range of samplers have been designed in the past, for quasi-Monte Carlo integration, rendering, image stippling, positionning objects or generally, to uniformly or non-uniformly cover some space. The generated samples can have various properties, such as being low discrepancy or stratified, having a blue noise spectrum, producing low integration error, with high packing density, satisfying a Poisson disk criterion, or high inter-point distances [Pharr et al. 2016; Singh et al. 2019]. Differentiability can also be desirable in contexts involving further optimizations, but may be problematic for specific samplers, for instance when considered in a differential renderer [Jakob et al. 2022b]. The large set of available samplers makes sample generation lacking genericity, with methods involving smooth non-convex optimization, integer linear programming, number theory, bruteforce approaches with clever data structures, etc. Finally, it may happen that sample distributions are known only through a set of examples, without a known dedicated sampler, hence the need for an example-based method able to generate point sets from a set of examples, while capturing the fine-grained properties of the point distribution.

Recently, diffusion models have become extremely popular in the context of image generation [Sohl-Dickstein et al. 2015; Ho et al. 2020; Rombach et al. 2022]. By learning how to denoise an image that initially only contains random values, these models have been able to produce impressive results, i.e., to learn the very fine structure of the manifold of realistic images. It hence seems judicious to take advantage of these models to learn the very fine structure of sample points produced by existing samplers. However, these models heavily rely on convolutions, which makes it impractical to efficiently handle point sets.

In this paper, we propose to learn the distribution of 2-d samples produced by a wide range of samplers using a diffusion model. When point sets are not stratified, we resort to an optimal transport matching to a uniform grid that mostly preserves neighborhood information so as to benefit from efficient convolutional layers. We demonstrate that a single architecture is able to learn sample

points produced by different methods, and even allows to reproduce non-uniform point sets. The differentiability of our network allows us to add properties to a given samplers, e.g., allowing to add low discrepancy properties to a given optimal transport-based sampler. We also demonstrate that a mild change in our architecture – adding distribution class conditioning – allows to train a single network for a whole set of samplers. Hence a single network can provide different types of point sets, and produce points of a desired distribution.

While our network is currently limited to generating 2-d or 3-d samples, it produces samples beyond the range of samples count it has been trained on. We provide trained networks alongside the paper and believe this exciting step will open the door to further applications. Code is provided in supplementary material.

## 2 RELATED WORKS

Existing samplers have a wide range of properties. We enumerate importants classes of samplers below.

*Blue Noise.* Blue noise samples have a characteristic "ring-like" Fourier power spectrum, with low frequencies converging to zero. They are interesting for Monte Carlo integration purposes [Subr and Kautz 2013; Pilleboue et al. 2015], digital halftoning [Ulichney 1987] or stippling [Deussen et al. 2000] and well describe arrangements of natural phenomenas that have been optimized through evolution such as the retinal distribution of cones [Yellott 1982]. They are often costly obtained through optimization, for instance using kernel approaches [Fattal 2011; Ahmed et al. 2022], pair-correlation function [Öztireli and Gross 2012] or optimal transport [De Goes et al. 2012; Qin et al. 2017; Paulin et al. 2020], though fast approximations exist [Nader and Guennebaud 2018]. Tile-based approaches pre-compute tiles for fast synthesis, but are memory demanding [Ostromoukhov et al. 2004; Ostromoukhov 2007; Ahmed et al. 2017; Kopf et al. 2006; Wachtel et al. 2014].

*Poisson Disk.* As an alternative way to tackle the blue noise point pattern construction and as coined by Ulichney [1987], Poisson disk samples have the property that no point fall within a distance smaller than a threshold from another point [Yuksel 2015; Gamito and Maddock 2009; Wei 2008; Bridson 2007; Dunbar and Humphreys 2006; Dippé and Wold 1985; Cook 1986]. Their spectra resemble those of blue noise distributions, except that they do not decrease towards zero as the frequency decreases [Pilleboue et al. 2015]. They naturally occur in other natural process such as the placement of trees in a forest. In low dimensions, they are relatively fast to compute.

*Low Discrepancy Sequences.* Discrepancy is a uniformity measure directly related to Monte Carlo integration error. Low discrepancy sequences (LDS) thus have several advantages. First they are sequences, so that samples can be progressively added. Second, they are low discrepancy, hence guaranteeing good numerical integration error [Niederreiter 1992; Lemieux 2009]. Samplers achieving low discrepancy usually rely on arithmetic and number theory constructions leading to extremely fast generators (*e.g.* in base 2, the $i$-th sample using [Sobol' 1967] is given by a matrix/vector multiplication in $GF(2)$ on the bitwise representation of $i$). Alternatively, lattices produce low discrepancy sequences. A rank-1 lattice repeatedly translates an initial point by a given amount in a given direction in a toric domain [Keller 2004]. Rank-n lattices similarly use multiple independent vectors. Good lattices can be similarly hard to optimize for [L'Ecuyer and Munger 2016].

*Designing Complex Point Processes.* Aside global point set properties such as blue-noise, Poisson disk or low discrepancy, the problem of designing a point process matching some exemplars or satisfying additional constraints has been addressed in several ways. One can design sampler mixing global properties such as low discrepancy and blue-noise [Ahmed et al. 2016; Ahmed and Wonka 2021; Perrier et al. 2018], or one can use a profile-based approach to generate LDS samplers with adjustable or with scriptable properties, such as blue-noise properties or stratification on some projections [Paulin et al. 2022; L'Ecuyer and Munger 2016]. Mixing point process properties can also be achieved by interpolating their high order statistics such as their pair-correlation functions [Öztireli and Gross 2012]. Focusing on spectral properties, Zhou et al. [2012] have proposed an energy formulation and a gradient descent approach to optimize samples targeting a given Fourier spectrum. Leimkühler et al. [2019] have followed a similar approach using a neural network to target specific profiles defined as combinations of radial power spectra. In a texture-synthesis like manner, Huang et al. [2022] proposed to extend point set patterns by using a set of Gabor filter results as input to a CNN and matching resulting feature maps. Tu et al. [2019] follow a similar approach of point pattern upscaling using irregular convolutions by evaluating the convolution operator on a grid. Targeting repetitive patterns, Roveri et al. [2015] use a multiscale local-global optimization that they applied repetitive point set synthesis.

*Point sets through deep learning.* Perhaps the closest to our work is that of Leimkühler et al. [2019]. They learn arbitrary dimensional point sets by matching point statistics such as power spectra or distance statistics. There is a number of important differences with respect to our work. First, they require statistics (e.g., a power spectrum) as input while we require examples from a given sampler. This allows us to capture all characteristics of samplers and not just selected statistics). Second, our network is able to produce point sets of significantly different sizes without re-training. Third, we propose a way to benefit from efficient convolutions on grids. While this restricts us to low-dimensional settings (we demonstrate our approach in two and three dimensions), this allows us to use thousands of convolution layers at different scales and to benefit from recent advances in diffusion models. These differences allow us to finely capture the structure of point sets (see Sec. 4.2). Point sets generated by our method can be used for Monte Carlo integration purposes. In this context, deep learning has been used to learn a control variate [Müller et al. 2020], though this does not directly address the location of point samples. Deep learning has also been used for importance sampling [Müller et al. 2019].

*Probabilistic Denoising Diffusion.* Our method is based on Probabilistic Denoising Diffusion, a concept introduced by Sohl-Dickstein et al. [2015] in the context of unsupervised learning. The core idea of denoising diffusion is to gradually remove any structure in an input image by progressively adding noise and to train a neural network to invert the degradation process. This allows to capture

the data distribution and sample from it. This idea has been extensively used for image synthesis [Ho et al. 2020] with impressive results, either by working directly in pixel space or in the latent space [Rombach et al. 2022]. Denoising diffusion models have been extended to 3D shape point sets, by conditioning on a shape latent using a PointNet encoder [Luo and Hu 2021], or by relying on a Point-Voxel CNN [Zhou et al. 2021]. A hierarchical approach combining both a global latent representation and a point latent representation using denoising diffusion models for both representation and Point-Voxel CNN for encoding and decoding the shape has also been proposed [Zeng et al. 2022]. While these architectures are able to sample coarse 3d shapes, and are related to our context since they address irregular data, they fail at capturing the fine-grained point distribution properties we are interested in. In this paper, we propose to exploit the capacity of these denoising diffusion models to learn structure from a set of examples to learn point distributions.

## 3 DENOISING DIFFUSION MODEL

### 3.1 Architecture

The denoising process involves a sequence of denoising operations which operate at given timesteps. Each denoising is achieved by a forward pass in a single denoising network $\varepsilon_\theta$, which takes as input both the noisy image $\tilde{x}_t$ and the embedded timestep $t$.

Our network architecture is very similar to the one of Ho et al. [2020]. It corresponds to a U-Net [Ronneberger et al. 2015], where each level is composed of two convolutional residual blocks (ResNet) and the feature maps are downsampled by a factor 2 between each level. While the original architecture included attention blocks between the convolutional blocks at some levels, we found that removing this attention led to comparable or better results and reduced the training time. We trained the model using 1000 diffusion time steps but used only 50 time steps at inference time, which allowed for faster synthesis for comparable results (see the supplementary material for an ablation study an our network architecture details).

The network learns a time-dependent noise model $\varepsilon_\theta(\tilde{x}_t, t)$ given a noise $\varepsilon_t$ added to the input data, $\tilde{x}_t = x_t + \varepsilon_t$ at each time step $t$. In our setting, $x_0$ is the offset between strata centers and the input point set as obtained in Sec 3.2. The network thus predicts noise, that can then be progressively removed from a gaussian white noise point set to denoise it according to the learned data distribution.

### 3.2 Convolutions on grids

While computing the required convolutions used in the diffusion model is possible on unstructured point sets [Groh et al. 2019; Simonovsky and Komodakis 2017; Hua et al. 2018], this comes at a prohibitive cost in our context, due to the large number of convolutions involved. Fortunately, our point sets are not arbitrary but may uniformly cover the unit square. In certain cases, they can be stratified, i.e., each stratum of size $\frac{1}{\sqrt{n}} \times \frac{1}{\sqrt{n}}$ contains a single sample. This is notably the case for the large class of $(0, m, s)$-nets samplers [Niederreiter 1992]. In that case, we use a pixel grid of $\sqrt{n} \times \sqrt{n}$ pixels, and store in each pixel the 2-d offset between the stratum center and its corresponding sample location. When this is not the case, we compute a linear assignment using optimal transport between the strata centers and the set of samples (Fig. 1) [Bonneel et al. 2011], and similarly store in each pixel the 2-d offset between the stratum center and its corresponding sample location. This assignment is done only once, upon loading a point set at training time, and is not needed at inference time. Doing so allows to work on 2-d grids and benefit from optimized convolutions. In our settings, the grid acts as an approximate nearest neighbor acceleration data structure, such that, when a convolution is performed, neighboring samples approximately correspond to neighboring pixels, and are thus appropriately weighted. We evaluate this property with non-uniform sampling in Sec. 4.3. This remapping further allows to remain invariant under re-ordering of samples. This encoding can be extended to point sets of any dimension following the same principle.

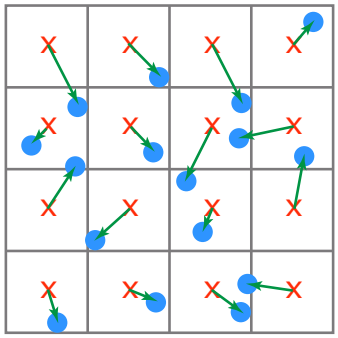

**Figure 1: When input point sets are not stratified, we compute a linear assignment problem between strata centers (red) and sample points (blue) using optimal transport. Each stratum stores its assigned point offset (green arrows). The grid thus serves as an approximate nearest neighbor acceleration data structure and benefits from efficient convolutions.**

### 3.3 Training

The benefit of a convolutional approach is that the same convolution weights can be used for different grid sizes. It thus becomes possible to train *the same* network with point sets of different sizes, and hope that it generalizes. We explore in Sec. 4.2 how it succeeds in generalizing. However, within a single batch, the sample count should remain the same, due to the way batches are processed. For a given batch of size $B$, we thus build a loss that sums contributions for different input grid sizes $\mathcal{S}$ stored in different batches:

$$\mathcal{L}(\epsilon_\theta, \epsilon_t) = \sum_{j \in \mathcal{S}} \frac{1}{B} \sum_{i=1}^{B} \|\epsilon_\theta(\tilde{x}_{t_i}, t_i) - \epsilon_{t_i}\|^2,$$

for randomly chosen $\{t_i\}$. We typically use $\mathcal{S} = \{8 \times 8, 16 \times 16, 32 \times 32\}$, hence learning from sample sizes $\{64, 256, 1024\}$. We obtain one trained network, of the same architecture but different training weights, per type of sampler, each able to produce point sets of different sample sizes.

### 3.4 Conditioning

Our vanilla architecture allows to learn the characteristics of a set of observations of sample distributions. However, it requires to train a different network for each distribution class. To alleviate this requirement, we propose a simple extension of our method to train a single network for several sampler classes. In practice, all pixels in the image are concatenated with a vector giving the encoding of the desired sampler class. See the supplementary material for more details and results.

## 4 VALIDATION AND APPLICATIONS

### 4.1 Implemenation

We train networks to reproduce Sobol' samples with Owen's scrambling [Sobol' 1967; Owen 1998] as a representative LDS matrix-based sampler, LatNetBuilder [L'Ecuyer and Munger 2016] samples as a representative LDS lattice-based sampler, a Poisson disk sampler (classical dart throwing approach), SOT [Paulin et al. 2020] as a representative blue noise sampler using optimal transport, GBN [Ahmed et al. 2022] as a representative kernel-based blue noise sampler, LDBN [Ahmed et al. 2016] as a sampler that combines low discrepancy properties and blue noise spectrum, and Rank-1 [Keller 2004] as a representative of lattice based sampler. We train all our models using 64k point sets of each sample count in $\mathcal{S}$, except for the SOT sampler trained with only 32 (*not 32k*) point sets to assess robustness to small training datasets. We train for a constant time of 3 hours, and synthesis time is typically 0.1s for a point set of 4096 points using 50 diffusion steps (2 seconds for 1000 diffusion steps) on an Nvidia V100. As a comparison, optimization-based samplers usually need several seconds to sample a point set of the same size (multithreaded CPU SOT and GPU-based GBN require 3.0s on AMD Ryzen 7 1700X and 4.5s on Nvidia V100 respectively). The source code is available at https://github.com/BDoignies/ExampleBasedSamplingWithDiffusion.

### 4.2 Properties of generated samples

We study power spectra, optimal transport energy, discrepancy, integration errors and minimum distance statistics of generated point sets, and verify that they match properties they were trained for. We also verify how our network generalizes as we increase the number of samples outside the range it was trained for. For these comparisons, we compare to the approach of Leimkühler et al. [2019] (DC for short in the graphs). For stationary and isotropic point processes (Poisson disk and GBN), we have used their publicly available implementation with a 1d radial mean power spectrum loss (same learning parameters as the one provided by the authors for similar experiments). Non-stationary or anisotropic point patterns (SOT, LDBN, Sobol'+Owen and Rank1), fall outside of the scope of the approach of Leimkühler et al. [2019] as it considers anisotropic samplers defined by isotropic properties on axis projections (for instance a 3d point set with blue-noise characteristics on the XY subspace and a step profile on the XZ subspace). We also include in our experiments a comparison to the Point Pattern synthesis approach [Huang et al. 2022] (PPS for short). This method being dedicated to point pattern upsampling, we use it to upscale point sets from 1024 samples to 4096. Additional upscaling results compared with Tu et al. [2019] are available in supplementary materials. On some violin plot figures we omit Sobol'+Owen or Rank1 as either their implementation fails to produce a point set, or the error values are above the others which would hinder the readability of the figure.

Finally, we have also tested point set dedicated denoising diffusion models [Luo and Hu 2021; Zhou et al. 2021] in Figure 2, showing that both methods fail at capturing the point distribution properties. The resulting point sets are very far from both the reference and our results.

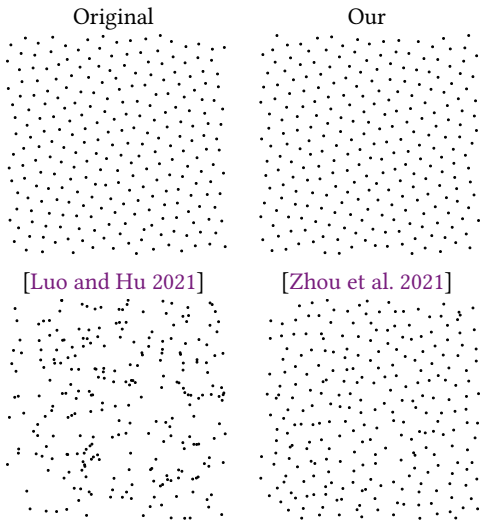


**Figure 2: Comparisons with alternative deep models dedicated to point cloud processing ([Luo and Hu 2021] and [Zhou et al. 2021]). For this experiment, we have considered an LDBN point set target with 256 samples.**

While we trained our network on small set of sample sizes ($\{64, 256, 1024\}$), we assess the performance of these metrics for other sample sizes ($\{576, 4096\}$). Its ability to generalize to unseen sample counts shows that our network did not merely memorize point sets from the training set. For most of these properties, we illustrate them with violin plots (Fig. 3, 4, 5, 6), that show the distribution of values in the form of vertical histograms (similar to a population pyramid). We compute them using 128 point sets.

*Power spectra.* In Fig. 13, we first show performances of the method of Leimkühler et al. [2019] and our approach to recover spectral properties of the training sets (either through 1d radial mean power spectra for stationay and isotropic point sets, or 2d spectra for other ones). As discussed above, capturing anisotropic spectra with the method of Leimkühler et al. [2019] is very challenging using a 2d spectra loss function. Our approach fully captures such characteristics.

*Optimal transport energy.* Optimal transport (OT) provides a way to characterize the uniformity of a point set by computing the (squared) semi-discrete optimal transport distance between the point set and a uniform distribution [Mérigot 2011]. Fig. 3 illustrates how we match the OT energy.

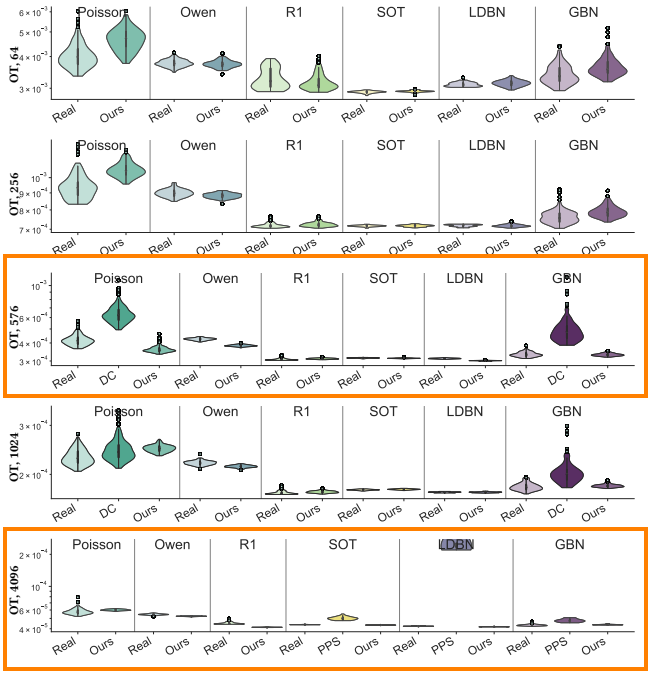


**Figure 3: We verify that the point sets predicted by our network match the semi-discrete optimal transport distance to a uniform distribution of the original point sets. These plots show these statistics distributions for 128 point sets from the training set and produced by our network, for sample counts of 64, 256, 576, 1024 and 4096 (top to bottom). The network has only been trained with point sets of 64, 256 and 1024 samples, but successfully predicts point sets of 576 and 4096 samples (results highlighted in an orange frame). Labels prefixed by DC refer to Deep Point Correlation [Leimkühler et al. 2019] (on 1d radial power spectral, unless 2d is specified), while NN refers to results produced by our Neural Network. We upsampled 1024 sample point sets to 4096 using the approach of Huang et al. [Huang et al. 2022] (PPS). For Owen, this resulted in values above our graph ranges. For R1, this produced NaN values.**

*Discrepancy and integration error.* Fig. 4 and 5 show how our network matches integration errors and discrepancy of point sets. For discrepancy, we used the generalized L2 discrepancy [Niederreiter 1992; Heinrich 1996]. For integration error, we compute the average MSE on the integration of wide anisotropic Gaussians (anisotropic ratio between 1:1 and 1:9, and Gaussian sizes ranging from 0.1 to 0.333 for its largest axis) or Heaviside distributions randomly linearly dividing the unit square. We randomly chose 64k integrands among 1 million, whose integral has been estimated with maximum precision as reference. These statistics also often match for sample sizes not seen during training ($\{576, 4096\}$).

*Minimum distance.* For distributions such as Poisson Disk, the minimum distance between any pair of samples can be important. We assess this statistics in Fig. 6. This property is highly sensitive as it only depends on the location of 2 points within the entire point set.

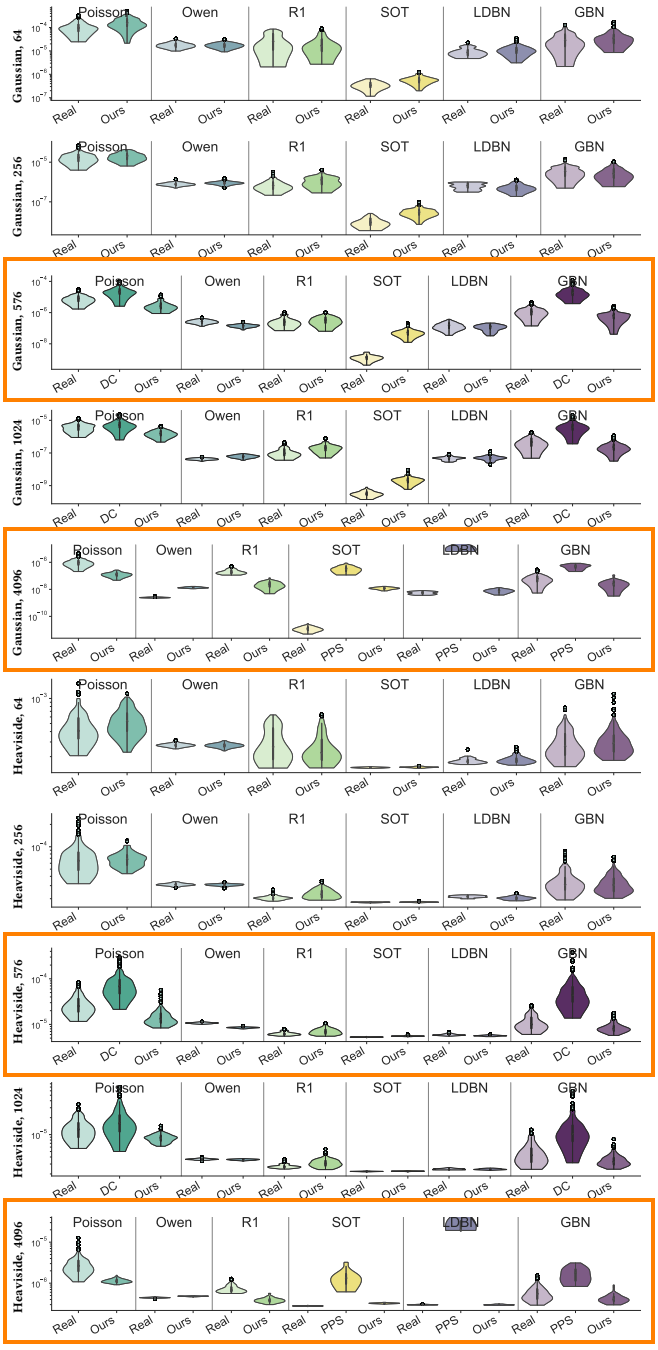


**Figure 4: Our network matches integration errors on Gaussian integrands (top 4 plots) and Heaviside integrands (bottom 4 plots), even beyond the sample sizes it was trained for ($\{64, 256, 1024\}$). Sample counts are 64, 256, 576, 1024 and 4096 (top to bottom for each integrand). For PPS, we upsampled 1024 sample point sets to 4096: for Owen, this resulted in values above our graph ranges; for R1 we obtained NaN values.**

For this property, the approach of Leimkühler et al. [2019] performs

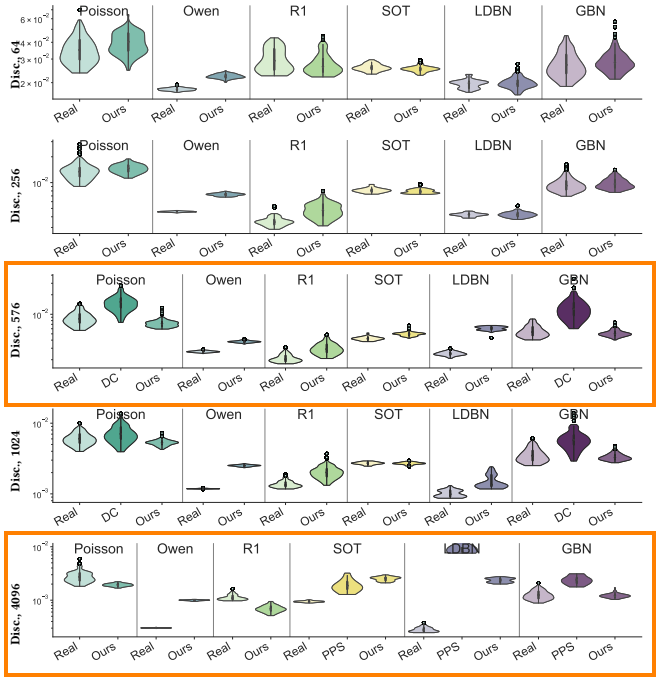


**Figure 5: Our network matches the generalized L2 discrepancy of the original point sets. Sample counts are 64, 256, 576, 1024 and 4096 (top to bottom). For PPS, we upsampled 1024 sample point sets to 4096: for Owen, this resulted in values above our graph ranges; for R1, this produced NaN values.**

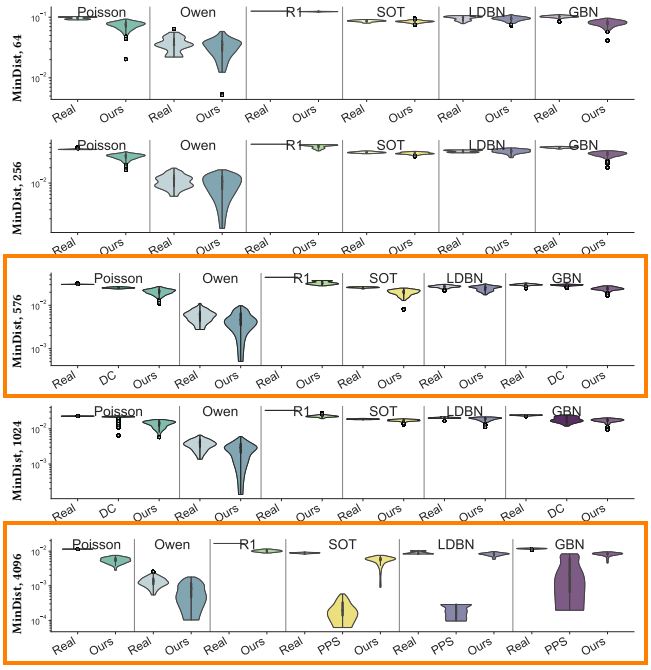


**Figure 6: We evaluate the minimum pairwise distance between samples. This property is highly sensitive as it only depends on the location of 2 samples. Our network tends to produce smaller values, while the sample repulsion of Leimkühler et al. [2019] better preserve minimum distances. Sample counts are 64, 256, 576, 1024 and 4096 (top to bottom). For PPS, we upsampled 1024 sample point sets to 4096: for Owen, this resulted in values above our graph ranges; for R1, this produced NaN values.**

remarkably well, due to the repulsion of points introduced during learning. In our approach, we tend to produce points with lower minimum distance value.

*Conditioning.* Finally, Fig. 7 evaluates the performances of the per class conditioning as discussed in Sect. 3.4. When compared to our vanilla model learned on each class, our conditioned model learned for all classes performs slightly worse than the vanilla models trained separately for each class, but it still provides a reasonable approximation. In the supplementary material, we provide further comparisons for all metrics and sample counts.

*Diffusion model in 3d.* Using optimal transport in 3d and convolutions on 3d grids, our model can be extended to process 3d point sets. In Fig. 8, a preliminary performance evaluation is given for the heaviside integration test on 4096 samples. Additional results are also given in supplementary material.

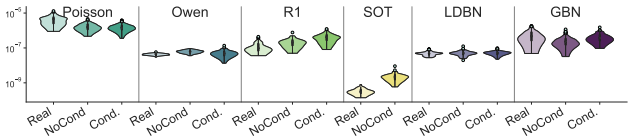


**Figure 7: We compare the vanilla per class trained model with the global conditioned one for the integration error metric on Gaussian integrands for 1024 samples.**

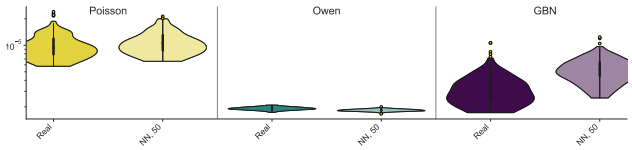


**Figure 8: Extension to 3D - Results of our network on integration errors for 3d Heaviside integrands and 4096 samples.**

## 4.3 Non-uniform distributions

The goal of our optimal transport matching to a uniform grid is to infer neighborhood information on the point sets from neighborhood information on the grid, that is, neighboring points on the grid are expected to correspond to neighboring samples. In Fig. 9, using a non-uniform linear ramp sliced optimal transport sampling, we show that, even for non-uniform sampling, our network successfully learns from examples and preserve spectral noise characteristics of the sampler. As a stress test, we also learn to sample a blobby function shown in Fig. 12. In this example, we learn from importance sampled GBN point sets obtained by rejection

sampling. Our network reproduces the sampling density well, and mostly preserves important characteristics of the GBN sampler despite inaccuracies in neighborhood information due to the grid embedding. As a failure case, for highly non-uniform point sets with many voids and clusters, *e.g.* pink noise of Fig. 10, the optimal transport matching may lead to suboptimal results. Clusters and voids in the pink noise distribution are located at different random locations in each training point set, which can render distribution learning more difficult. Our approach thus fails when the local density of samples varies among examples of the training set.

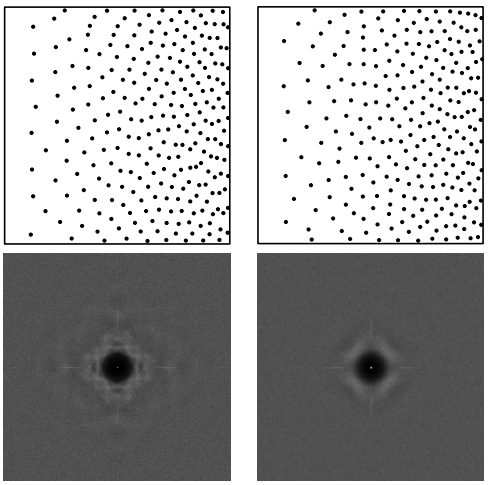

**Figure 9: We sample from a learned sliced OT linear ramp. Top row, left. One example point set used for training (among 66,035). Top row, right. One synthesized point set. Bottom row. Unwarping example and synthesized point sets to recover a uniform distribution shows that their spectra match. The uniformity of the unwarped samples can also be measured: the semi-discrete optimal transport energy averaged for 128 realizations of 256 samples is $7.24.10^{-4}$ for the neural network output, compared with $7.16.10^{-4}$ for the original sliced OT uniform samples.**

## 4.4 Application to constrained point set optimization

Aside from the fast generation of point sets, we also benefit from the differentiability of our network to further optimize point sets within their class.

We illustrate how the differentiability of our network can be used to add properties to generated point sets. Here, we wish to add low discrepancy properties to a sliced optimal transport sampler [Paulin et al. 2020], to benefit from both low discrepancy and low optimal transport energy. This is made feasible since our network is differentiable and produces point sets of a single class it is trained from. First, we train the network on SOT point sets and then freeze the weights of the network. Next, we optimize the input gaussian noise offset grid such that the synthesized point set minimizes the L2 discrepancy while the network ensures that it remains SOT-like. As backpropagation requires significant memory

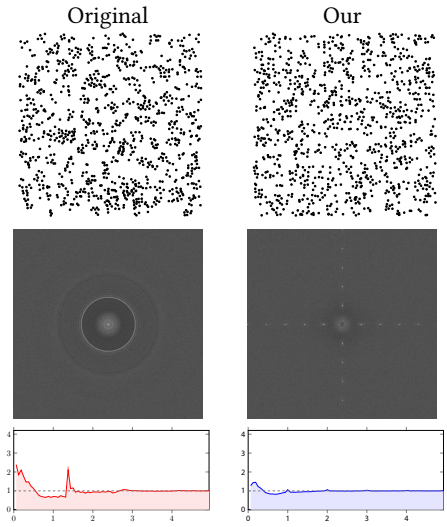


**Figure 10: On a higly non-uniform pink noise point pattern (128 realizations of 1024 samples), our approach can only capture partial properties of the point pattern.**

overhead, we reduce the number of diffusion steps to 100 (instead of 1000) in the diffusion model. In Fig. 11, we illustrate the result of our optimization in terms of discrepancy and optimal transport energy, and illustrate with an example generated point set.

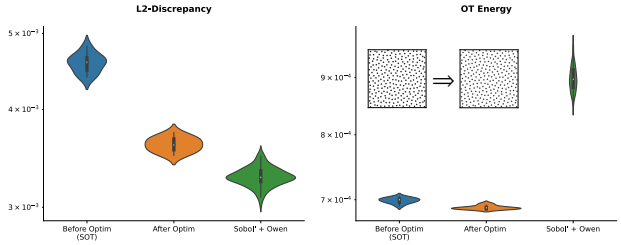


**Figure 11: We used a trained SOT sampling network to optimize the discrepancy of the generated point sets among the class of SOT point sets. We illustrate the OT energy and discrepancy value for 10 point sets before and after the optimization process and show Sobol' + Owen as reference value for both metrics. After the optimization, discrepancy matches that of Sobol' + Owen while retaining OT energy properties of SOT sampler.**

## 5 DISCUSSIONS & PERSPECTIVES

We showed that diffusion models provide a powerful tool for learning how to generate point sets directly from examples across a wide range of samplers and they generalize well with sample size. Generalization hints at the fact that the network is correctly learning the general principles that make each point set so particular. The capacity of our network to produce possibly non-uniform example-based point sets may open the door to syntheses where sampling data are only available through a small number of measurements (e.g.,

distribution of trees, cells, etc.) and optimizing only for summarized statistics (power spectrum or PCF) is not desired. This is a promising direction as we have successfully trained our network with 32 examples of each class (see supplementary material). Another promising direction lies in other types of network conditioning, such as property conditioning. Such a model would allow the user to specify numerical values for all or a subset of well-chosen properties (discrepancy, minimum distance, spectra...) and the network would design a point set fitting these properties. However, this would require heavy architecture changes and we leave it as a possible future work.

While in principle our method would work in arbitrary dimension, the efficiency gained through our convolutions on grids would be lost as storing higher dimensional grids becomes impractical, both in terms of storage (that exponentially grows with dimension) and supported sample size (in the form $k^d$ for some $k$, similarly to stratified samplers). To date, higher dimensional data would be better supported by the approach of Leimkühler et al. [2019] that does not rely on grids. Still, we believe our use of optimal transport matching for adapting a widespread convolutional network to the unstructured setting could benefit other low-dimensional applications.

In the settings we focus on, in most cases our samples preserve characteristics of major samplers well, including their power spectrum, Monte Carlo integration quality, distance statistics, optimal transport energy and discrepancy. Our diffusion-based sampler allows to generate point sets much faster than some optimization-based samplers by learning from their output. However, sampling speed remains an issue for time-critical applications, notably compared to fast samplers such as Sobol' or LDBN. Aside for the fast generation of diverse point sets, we have shown use for our network's differentiability by adding a low discrepancy property to an optimal transport-based sampler. Rendering applications could benefit from our samplers, e.g., through differentiable rendering pipelines [Jakob et al. 2022a] or for generating point sets nicely distributing Monte Carlo error in a blue noise fashion in screen space [Salaün et al. 2022].

## ACKNOWLEDGMENTS

This work was partially funded by ANR-20-CE45-0025 (MoCaMed) and gifts from Adobe Inc. We gratefully acknowledge support from the CNRS/IN2P3 Computing Center (Lyon - France) for providing computing and data-processing resources needed for this work.This work was granted access to the HPC/AI resources of IDRIS under the allocation 2022-AD011012547R1 made by GENCI.

## REFERENCES

Abdalla G. M. Ahmed, Till Niese, Hui Huang, and Oliver Deussen. 2017. An Adaptive Point Sampler on a Regular Lattice. *ACM Trans. Graph.* 36, 4 (July 2017), 138:1–138:13. https://doi.org/10.1145/3072959.3073588

Abdalla G. M. Ahmed, Hélène Perrier, David Coeurjolly, Victor Ostromoukhov, Jianwei Guo, Dong-Ming Yan, Hui Huang, and Oliver Deussen. 2016. Low-Discrepancy Blue Noise Sampling. *ACM Trans. on Graphics (SIGGRAPH Asia)* 35, 6 (2016), 247:1–247:13. https://doi.org/f9cpt2

Abdalla G. M. Ahmed, Jing Ren, and Peter Wonka. 2022. Gaussian Blue Noise. *ACM Trans. Graph.* 41, 6, Article 260 (nov 2022), 15 pages. https://doi.org/jtp8

Abdalla G. M. Ahmed and Peter Wonka. 2021. Optimizing Dyadic Nets. *ACM Trans. on Graphics (SIGGRAPH)* 40, 4 (2021), 141:1–141:17. https://doi.org/hn22

Michael Balzer, Thomas Schlömer, and Oliver Deussen. 2009. Capacity-Constrained Point Distributions: A Variant of Lloyd's Method. *ACM Trans. Graph.* 28, 3, Article 86 (jul 2009), 8 pages. https://doi.org/10.1145/1531326.1531392

Nicolas Bonneel, Michiel Van De Panne, Sylvain Paris, and Wolfgang Heidrich. 2011. Displacement interpolation using Lagrangian mass transport. In *Proceedings of the 2011 SIGGRAPH Asia conference*. 1–12. https://doi.org/gkcqgt

Robert Bridson. 2007. Fast Poisson disk sampling in arbitrary dimensions. *SIGGRAPH sketches* 10, 1 (2007), 1. https://doi.org/gf8tsr

R. Dennis Cook. 1986. Assessment of Local Influence. *Journal of the Royal Statistical Society: Series B (Methodological)* 48, 2 (1986), 133–155. https://doi.org/10.1111/j.2517-6161.1986.tb01398.x arXiv:https://rss.onlinelibrary.wiley.com/doi/pdf/10.1111/j.2517-6161.1986.tb01398.x

Fernando De Goes, Katherine Breeden, Victor Ostromoukhov, and Mathieu Desbrun. 2012. Blue noise through optimal transport. *ACM Trans. Graph.* 31, 6 (2012), 171:1–171:10. https://doi.org/gbb6n9

Oliver Deussen, Stefan Hiller, Cornelius Overveld, and Thomas Strothotte. 2000. Floating Points: A Method for Computing Stipple Drawings. *Computer Graphics Forum (EG'00)* 19, 3 (2000), 40–51. https://doi.org/fg9w98

Mark A. Z. Dippé and Erling Henry Wold. 1985. Antialiasing through Stochastic Sampling. In *Proceedings of the 12th Annual Conference on Computer Graphics and Interactive Techniques (SIGGRAPH '85)*. Association for Computing Machinery, New York, NY, USA, 69–78. https://doi.org/10.1145/325334.325182

Daniel Dunbar and Greg Humphreys. 2006. A spatial data structure for fast Poisson-disk sample generation. *ACM Transactions on Graphics (TOG)* 25, 3 (2006), 503–508.

Raanan Fattal. 2011. Blue-Noise Point Sampling Using Kernel Density Model. *ACM Trans. Graph.* 30 (2011), 48:1–48:12. https://doi.org/cv7pbv

Manuel N Gamito and Steve C Maddock. 2009. Accurate multidimensional Poisson-disk sampling. *ACM Trans. Graph.* 29, 1 (2009), 8:1–8:19. https://doi.org/dr8646

Fabian Groh, Patrick Wieschollek, and Hendrik PA Lensch. 2019. Flex-Convolution: Million-scale point-cloud learning beyond grid-worlds. In *Computer Vision–ACCV 2018: 14th Asian Conference on Computer Vision, Perth, Australia, December 2–6, 2018, Revised Selected Papers, Part I 14*. Springer, 105–122.

Stefan Heinrich. 1996. Efficient algorithms for computing the L2-discrepancy. *Math. Comp.* 65, 216 (1996), 1621–1633.

Jonathan Ho, Ajay Jain, and Pieter Abbeel. 2020. Denoising diffusion probabilistic models. *Advances in Neural Information Processing Systems* 33 (2020), 6840–6851.

Binh-Son Hua, Minh-Khoi Tran, and Sai-Kit Yeung. 2018. Pointwise convolutional neural networks. In *Proceedings of the IEEE conference on computer vision and pattern recognition*. 984–993.

Xingchang Huang, Pooran Memari, Hans-Peter Seidel, and Gurprit Singh. 2022. Point-Pattern Synthesis using Gabor and Random Filters. In *Computer Graphics Forum*, Vol. 41. Wiley Online Library, 169–179.

Wenzel Jakob, Sébastien Speierer, Nicolas Roussel, Merlin Nimier-David, Delio Vicini, Tizian Zeltner, Baptiste Nicolet, Miguel Crespo, Vincent Leroy, and Ziyi Zhang. 2022b. *Mitsuba 3 renderer*. https://mitsuba-renderer.org

Wenzel Jakob, Sébastien Speierer, Nicolas Roussel, and Delio Vicini. 2022a. Dr.Jit: A Just-In-Time Compiler for Differentiable Rendering. *ACM Trans. on Graphics (SIGGRAPH)* 41, 4 (2022), 124:1–124:19. https://doi.org/gqjn7p

Alexander Keller. 2004. Stratification by rank-1 lattices. In *Monte Carlo and Quasi-Monte Carlo Methods 2002*, Harald Niederreiter (Ed.). Springer, 299–313. https://doi.org/fks8z8

Johannes Kopf, Daniel Cohen-Or, Oliver Deussen, and Dani Lischinski. 2006. Recursive Wang Tiles for Real-Time Blue Noise. *ACM Trans. Graph.* 25, 3 (2006), 509–518. https://doi.org/dgvw52

Pierre L'Ecuyer and David Munger. 2016. LatticeBuilder: A General Software Tool for Constructing Rank-1 Lattice Rules. *ACM Transactions on Mathematical Software* 42 (2016), 1–30. https://doi.org/10.1145/2754929

Thomas Leimkühler, Gurprit Singh, Karol Myszkowski, Hans-Peter Seidel, and Tobias Ritschel. 2019. Deep point correlation design. *ACM Trans. on Graphics (SIGGRAPH Asia)* 38, 6 (2019), 1–17. https://doi.org/ggfg2x

Christiane Lemieux. 2009. *Monte Carlo and Quasi-Monte Carlo Sampling*. Springer. https://doi.org/b8r4z5

Shitong Luo and Wei Hu. 2021. Diffusion probabilistic models for 3d point cloud generation. In *Proceedings of the IEEE/CVF Conference on Computer Vision and Pattern Recognition*. 2837–2845.

Quentin Mérigot. 2011. A multiscale approach to optimal transport. In *Computer Graphics Forum*, Vol. 30. Wiley Online Library, 1583–1592. https://doi.org/cjh4q8

Thomas Müller, Brian McWilliams, Fabrice Rousselle, Markus Gross, and Jan Novák. 2019. Neural importance sampling. *ACM Trans. on Graphics* 38, 5 (2019), 1–19. https://doi.org/jtrf

Thomas Müller, Fabrice Rousselle, Alexander Keller, and Jan Novák. 2020. Neural control variates. *ACM Transactions on Graphics (TOG)* 39, 6 (2020), 1–19. https://doi.org/jtrj

Georges Nader and Gael Guennebaud. 2018. Instant transport maps on 2D grids. *ACM Trans. Graph.* 37, 6 (2018), 249:1–249:13. https://doi.org/jtrg

Harald Niederreiter. 1992. *Random Number Generation and Quasi-Monte Carlo Methods*. Society for Industrial and Applied Mathematics (SIAM), Philadelphia, PA, USA. https://doi.org/fd5fjw

Victor Ostromoukhov. 2007. Sampling with polyominoes. In *ACM Trans. Graph.*, Vol. 26. ACM, 78.

Victor Ostromoukhov, Charles Donohue, and Pierre-Marc Jodoin. 2004. Fast Hierarchical Importance Sampling with Blue Noise Properties. *ACM Trans. on Graphics (SIGGRAPH)* 23, 3 (2004), 488–495.

Art B. Owen. 1998. Scrambling Sobol' and Niederreiter–Xing Points. *Journal of Complexity* 14, 4 (1998), 466–489.

Cengiz Öztireli and Markus Gross. 2012. Analysis and synthesis of point distributions based on pair correlation. *ACM Transactions on Graphics (TOG)* 31, 6 (2012), 1–10. https://doi.org/gbb6qr

Loïs Paulin, Nicolas Bonneel, David Coeurjolly, Jean-Claude Iehl, Alexander Keller, and Victor Ostromoukhov. 2022. MatBuilder: Mastering Sampling Uniformity over Projections. *ACM Trans. on Graphics (SIGGRAPH)* 41, 4 (2022), 84:1–84:13. https://github.com/loispaulin/matbuilder

Loïs Paulin, Nicolas Bonneel, David Coeurjolly, Jean-Claude Iehl, Antoine Webanck, Mathieu Desbrun, and Victor Ostromoukhov. 2020. Sliced optimal transport sampling. *ACM Trans. on Graphics (SIGGRAPH)* 39, 4 (2020), 99:1–99:17. https://doi.org/gg8xfj

Hélène Perrier, David Coeurjolly, Feng Xie, Matt Pharr, Pat Hanrahan, and Victor Ostromoukhov. 2018. Sequences with Low-Discrepancy Blue-Noise 2-D Projections. 37, 2 (2018), 339–353. https://doi.org/gd2j2d

Matt Pharr, Wenzel Jakob, and Greg Humphreys. 2016. *Physically Based Rendering: From Theory to Implementation* (3 ed.). Morgan-Kaufmann.

Adrien Pilleboue, Gurprit Singh, David Coeurjolly, Michael Kazhdan, and Victor Ostromoukhov. 2015. Variance Analysis for Monte Carlo Integration. *ACM Trans. Graph.* 34, 4 (2015), 124:1–124:14. https://doi.org/f7m28c

Hongxing Qin, Yi Chen, Jinlong He, and Baoquan Chen. 2017. Wasserstein Blue Noise Sampling. *ACM Trans. Graph.* 36, 4, Article 137a (Oct. 2017). https://doi.org/gcj3d3

Robin Rombach, Andreas Blattmann, Dominik Lorenz, Patrick Esser, and Björn Ommer. 2022. High-Resolution Image Synthesis with Latent Diffusion Models. In *Proceedings of the IEEE Conference on Computer Vision and Pattern Recognition (CVPR)*. 10684–10695.

Olaf Ronneberger, Philipp Fischer, and Thomas Brox. 2015. U-net: Convolutional networks for biomedical image segmentation. In *International Conference on Medical image computing and computer-assisted intervention*. Springer, 234–241. https://doi.org/gcgk7j

Riccardo Roveri, A Cengiz Öztireli, Sebastian Martin, Barbara Solenthaler, and Markus Gross. 2015. Example based repetitive structure synthesis. In *Computer Graphics Forum*, Vol. 34. Wiley Online Library, 39–52.

Corentin Salaün, Iliyan Georgiev, Hans-Peter Seidel, and Gurprit Singh. 2022. Scalable Multi-Class Sampling via Filtered Sliced Optimal Transport. *ACM Trans. Graph.* 41, 6, Article 261 (nov 2022), 14 pages. https://doi.org/10.1145/3550454.3555484

Adrian Secord. 2002. Weighted Voronoi Stippling. In *Proceedings of the 2nd International Symposium on Non-Photorealistic Animation and Rendering* (Annecy, France) *(NPAR '02)*. Association for Computing Machinery, New York, NY, USA, 37–43. https://doi.org/10.1145/508530.508537

Martin Simonovsky and Nikos Komodakis. 2017. Dynamic edge-conditioned filters in convolutional neural networks on graphs. In *Proceedings of the IEEE conference on computer vision and pattern recognition*. 3693–3702.

Gurprit Singh, Cengiz Öztireli, Abdalla G. M. Ahmed, David Coeurjolly, Kartic Subr, Oliver Deussen, Victor Ostromoukhov, Ravi Ramamoorthi, and Wojciech Jarosz. 2019. Analysis of sample correlations for Monte Carlo rendering. In *Computer Graphics Forum*, Vol. 38. Wiley Online Library, 473–491.

Ilya M. Sobol'. 1967. On the distribution of points in a cube and the approximate evaluation of integrals. *Zhurnal Vychislitel'noi Matematiki i Matematicheskoi Fiziki* 7, 4 (1967), 784–802. https://doi.org/crdj6j

Jascha Sohl-Dickstein, Eric Weiss, Niru Maheswaranathan, and Surya Ganguli. 2015. Deep unsupervised learning using nonequilibrium thermodynamics. In *International Conference on Machine Learning*. PMLR, 2256–2265.

Kartic Subr and Jan Kautz. 2013. Fourier analysis of stochastic sampling strategies for assessing bias and variance in integration. *ACM Trans. Graph.* 32, 4, Article 128 (2013), 12 pages. https://doi.org/gbdg7c

Peihan Tu, Dani Lischinski, and Hui Huang. 2019. Point Pattern Synthesis via Irregular Convolution. In *Computer Graphics Forum*, Vol. 38. Wiley Online Library, 109–122.

Robert Ulichney. 1987. *Digital Halftoning*. MIT Press, Cambridge, MA, USA.

Florent Wachtel, Adrien Pilleboue, David Coeurjolly, Katherine Breeden, Gurprit Singh, Gaël Cathelin, Fernando De Goes, Mathieu Desbrun, and Victor Ostromoukhov. 2014. Fast tile-based adaptive sampling with user-specified Fourier spectra. *ACM Trans. on Graphics (SIGGRAPH)* 33, 4 (2014), 1–11. https://doi.org/f6cz6k

Li-Yi Wei. 2008. Parallel Poisson disk sampling. In *ACM Trans. Graph.*, Vol. 27. ACM, 20. https://doi.org/cs3jjv

John I. Yellott. 1982. Spectral analysis of spatial sampling by photoreceptors: Topological disorder prevents aliasing. *Vision Research* 22, 9 (1982), 1205 – 1210. https://doi.org/fsgtr4

Cem Yuksel. 2015. Sample elimination for generating Poisson disk sample sets. In *Computer Graphics Forum*, Vol. 34. Wiley Online Library, 25–32. https://doi.org/f7k7c7

Xiaohui Zeng, Arash Vahdat, Francis Williams, Zan Gojcic, Or Litany, Sanja Fidler, and Karsten Kreis. 2022. LION: Latent Point Diffusion Models for 3D Shape Generation. In *Advances in Neural Information Processing Systems (NeurIPS)*.

Linqi Zhou, Yilun Du, and Jiajun Wu. 2021. 3d shape generation and completion through point-voxel diffusion. In *Proceedings of the IEEE/CVF International Conference on Computer Vision*. 5826–5835.

Yahan Zhou, Haibin Huang, Li-Yi Wei, and Rui Wang. 2012. Point sampling with general noise spectrum. *ACM Trans. Graph.* 31, 4 (2012), 76.

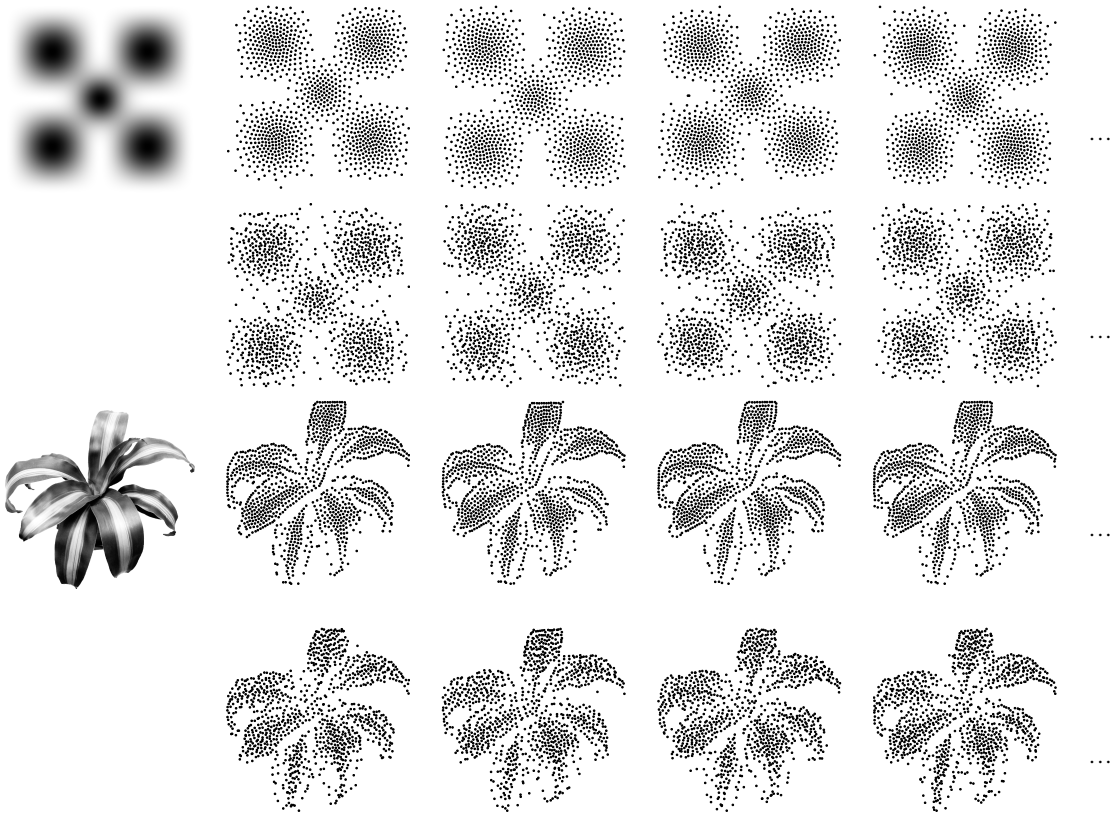

**Figure 12: As a stress test, we sample 1024 points from the density $0.2e^{-20(x^2+y^2)} + 0.2\sin(\pi x)^2\sin(\pi y)^2$ [Balzer et al. 2009] by importance sampling using 256 GBN stippling pointset as a training set (first row). Our sampler reproduces the density well and mostly preserves important characteristics of the sampler (second row). We also illustrate an image stippling experiment (1024 samples, trained using GBN stippling, image from [Secord 2002]).**

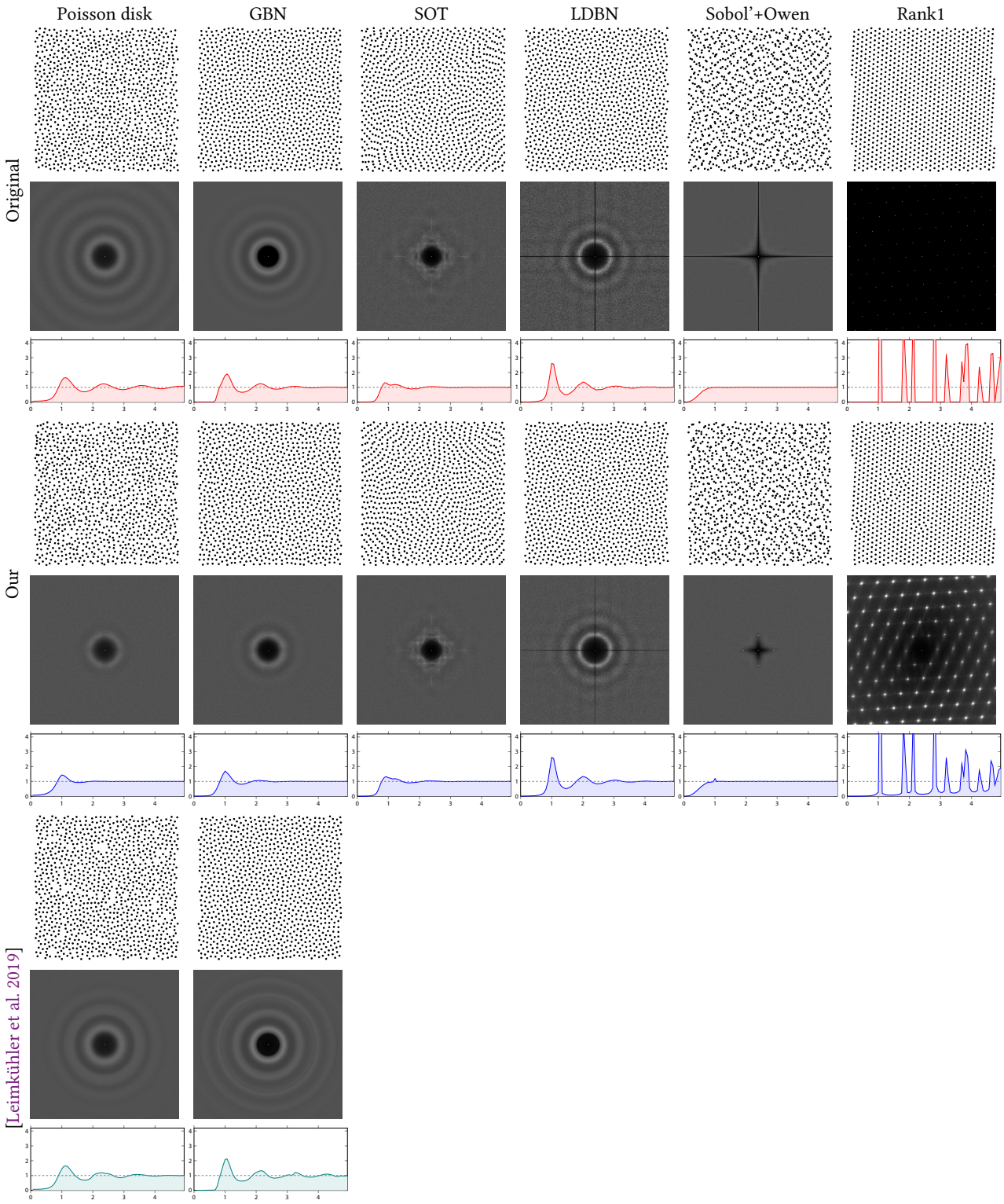


**Figure 13: For various input samplers and their spectral content (Fourier power spectrum and radial mean power spectrum), we compare our approach (last three rows) with that of Leimkühler et al. [2019] (1d radial mean power spectrum loss for Poisson disk and GBN).**

# Supplementary material for Example-Based Sampling with Diffusion Models


Bastien Doignies
Univ Lyon, UCBL, CNRS, INSA Lyon, LIRIS
France
bastien.doignies@liris.cnrs.fr

Nicolas Bonneel
Univ Lyon, CNRS, UCBL, INSA Lyon, LIRIS
France
nicolas.bonneel@liris.cnrs.fr

David Coeurjolly
Univ Lyon, CNRS, UCBL, INSA Lyon, LIRIS
France
david.coeurjolly@liris.cnrs.fr

Julie Digne
Univ Lyon, CNRS, UCBL, INSA Lyon, LIRIS
France
julie.digne@liris.cnrs.fr

Lois Paulin
Univ Lyon, UCBL, CNRS, INSA Lyon, LIRIS, Adobe
France
paulin@adobe.com

Jean-Claude Iehl
Univ Lyon, UCBL, CNRS, INSA Lyon, LIRIS
France
jean-claude.iehl@liris.cnrs.fr

Victor Ostromoukhov
Univ Lyon, UCBL, CNRS, INSA Lyon, LIRIS
France
victor.ostromoukhov@liris.cnrs.fr



**ACM Reference Format:**
Bastien Doignies, Nicolas Bonneel, David Coeurjolly, Julie Digne, Lois Paulin, Jean-Claude Iehl, and Victor Ostromoukhov. 2023. Supplementary material for Example-Based Sampling with Diffusion Models. In *Proceedings of SIGGRAPH Asia 2023 Conference Papers (SA Conference Papers '23).* ACM, New York, NY, USA, 22 pages. https://doi.org/10.1145/nnnnnnn.nnnnnnn


Contents



## 1 DIFFUSION MODEL

Diffusion models date back to the work of Sohl-Dickstein et al. [2015] but were popularized by Ho et al. [2020] for image synthesis. This section recalls the details for completeness.

Probabilistic Denoising Diffusion models involve a *forward* process, where noise is gradually added to the signal (here an image) and a *reverse* process where noise is removed through a learnable network. The forward diffusion process is a Markov Chain, where each transition adds Gaussian Noise to the image, following:

$$q(x_t|x_{t-1}) = \mathcal{N}(x_t; \sqrt{1-\beta_t}x_{t-1}, \beta_t I)\,, \tag{1}$$

where $(\beta_t)_{t=0}^T$ are the noise variances for each time $t$. The variance schedule is chosen such that nothing distinguishes $x_T$ from a white noise. In our model, we set the variances $\beta_t$ to follow a linear schedule.

One has:

$$q_{x_1:T|x_0} = \prod_{t=1\cdots T} q(x_t|x_{t-1})\,. \tag{2}$$

The reverse (denoising) process is also a Markov Chain, with transitions:

$$p_\theta(x_{t-1}|x_t) = \mathcal{N}(x_{t-1}; \mu_\theta(x_t,t), \Sigma_\theta(x_t,t))\,, \tag{3}$$

$\mu_\theta$ and $\Sigma_\theta$ are learned by examples. To simplify, following the work of Ho et al. [2020], we consider that $\Sigma_\theta = \sigma_t I$, with $\sigma_t = \beta_t$. The forward process allows to sample $x_t$ with arbitrary $t$ from $x_0$, following:

$$q(x_t|x_0) = \mathcal{N}(x_t; \sqrt{\bar{\alpha}_t}x_0, (1-\bar{\alpha}_t)I)\,, \tag{4}$$

with $\alpha_t = 1-\beta_t$ and $\bar{\alpha}_t = \prod_{s=1}^t \alpha_s$.

During training, and image $x_0$ is drawn from the set of examples, along with a random time $t \in 1\cdots T$, a random noise image $\varepsilon$ is drawn following $\mathcal{N}(0, I)$ and the algorithm tries to minimize:

$$\|\varepsilon - \varepsilon_\theta(\sqrt{\bar{\alpha}_t}x_0 + \sqrt{1-\alpha_t}\varepsilon, t)\|^2\,, \tag{5}$$

by gradient descent.

During sampling a random noise image $z \sim \mathcal{N}(0, I)$ is drawn and iteratively denoised by applying:

$$x_{t-1} = \frac{1}{\sqrt{\bar{\alpha}_t}}(x_t - \frac{1-\alpha_t}{\sqrt{1-\bar{\alpha}_t}}\varepsilon_\theta(x_t,t)) + \sigma_t z\,, \tag{6}$$


*SA Conference Papers '23, December 12–15, 2023, Sydney, NSW, Australia*

where $z$ is a random noise and in our case, we take $\sigma_t = \beta_t$ The key ingredient of diffusion models is the approximator $\epsilon_\theta$, which is modeled by a neural network.

## 2 NETWORK

Our network is a slightly modified version of the denoising network of Ho et al. [2020] and is summarized on Figure 1.As for hyperparameters, we used a fixed linear variance schedule from $10^{-4}$ to $10^{-2}$ with 1000 diffusion steps at training, similarly to Ho et al. [2020].

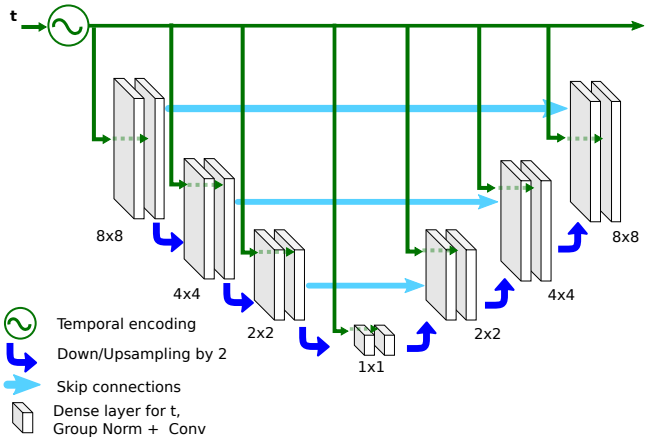


**Figure 1: Denoising network architecture**

*Class conditioned variant.* We also introduce a modified network able to learn multiple classes by conditioning it with the name of the distribution class. To do so, we encode the class through one hot encoding followed by an MLP, whose parameters are learned together with the denoising network parameters. All pixels in the input noise image are then concatenated with the resulting vector. Note that the condition vector is constant over the whole image since it encodes the class of the desired sample distribution.

## 3 ADDITIONAL UPSCALING COMPARISONS TO [Huang et al. 2022] AND [Tu et al. 2019]

In Figure 2, we provide additional upscaling results to 4096 samples using Huang et al. [2022] and Tu et al. [2019] when targeting an Sobol'+Owen point pattern. Both Huang et al. [2022] and Tu et al. [2019] are not able to upsample the point set while preserving the statistical properties. On the contrary, our approach provides a much more reliable upsampling.

## 4 COMPLETE EVALUATION OF THE CLASS CONDITIONED VARIANT

In Figures 3, 4, 5, 6, 7, we compare, for all metrics, the class conditioned variant (*i.e.* trained on all classes with conditioning) with the results obtained by single trained class models. While the class conditioned model performs slightly worse than our per class vanilla architecture, the various metrics show that it is still a good approximation of the various samplers. The most difficult property to capture seems to be the generalized L2 discrepancy of the distribution, but even so, the conditioned model is not too far from the per class model.

## 5 ADDITIONAL RESULTS IN 3D

In Figures 8, 9, 10, 11 and 12, we provide additional preliminary results for 3d point set synthesis using our network. Our model successfully captures key properties of the learned point sets.

## 6 ABLATION STUDY: NUMBER OF DIFFUSION STEPS

In Figures 3, 4, 5, 6, 7, we compare, for all metrics, the quality of our model when changing the number of diffusion steps in {50, 100, 250, 500, 1000} when generating the point sets (the learning stage is still performed with 1000 diffusion steps). The inference computational cost is linear with the number of steps, and we have observed that using only 50 steps is a good trade-off between quality and efficiency.

## 7 ABLATION STUDY: EFFECT OF THE DATABASE SIZE

As discussed in the main paper, the number of examplars used for the training may have an impact on the model quality. In figures 18, 19, 20, 21 and 22, we compare for all metrics the quality of the proposed model on a training set of 64k realizations and a training set of 32 realizations. The model seems to perform well as reported by the computed metrics, but further experiments would be necessary to assess the generalization power of the model trained on 32-examples datasets.

## REFERENCES

Jonathan Ho, Ajay Jain, and Pieter Abbeel. 2020. Denoising diffusion probabilistic models. *Advances in Neural Information Processing Systems* 33 (2020), 6840–6851.

Xingchang Huang, Pooran Memari, Hans-Peter Seidel, and Gurprit Singh. 2022. Point-Pattern Synthesis using Gabor and Random Filters. In *Computer Graphics Forum*, Vol. 41. Wiley Online Library, 169–179.

Jascha Sohl-Dickstein, Eric Weiss, Niru Maheswaranathan, and Surya Ganguli. 2015. Deep unsupervised learning using nonequilibrium thermodynamics. In *International Conference on Machine Learning*. PMLR, 2256–2265.

Peihan Tu, Dani Lischinski, and Hui Huang. 2019. Point Pattern Synthesis via Irregular Convolution. In *Computer Graphics Forum*, Vol. 38. Wiley Online Library, 109–122.

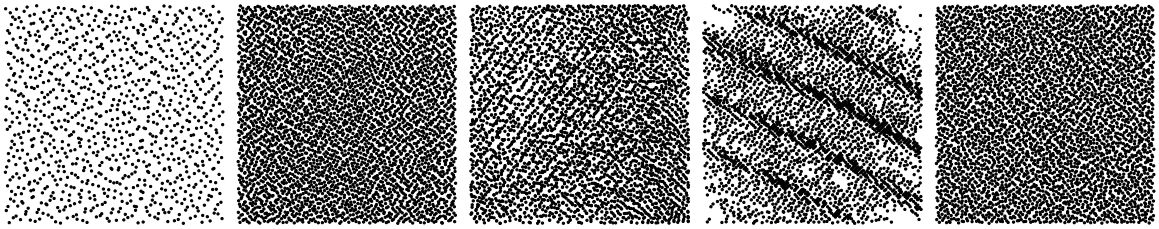

(a) Sobol'+Owen (1k) (b) Sobol'+Owen (4k) (c) [Huang et al. 2022] (d) [Tu et al. 2019] (e) Ours

**Figure 2: Using a 1024 Sobol'+Owen realization (a), we use Huang et al. [2022] (*c*), and [Tu et al. 2019] (*d*), to generate a 4096 point set. Finally, (*e*) presents our result (refer to the main paper for quantitative comparisons. Note that the 4096 Sobol'+Owen point set (*b*) is just given as a reference, the Owen scrambling differs from the one used for (*a*).**

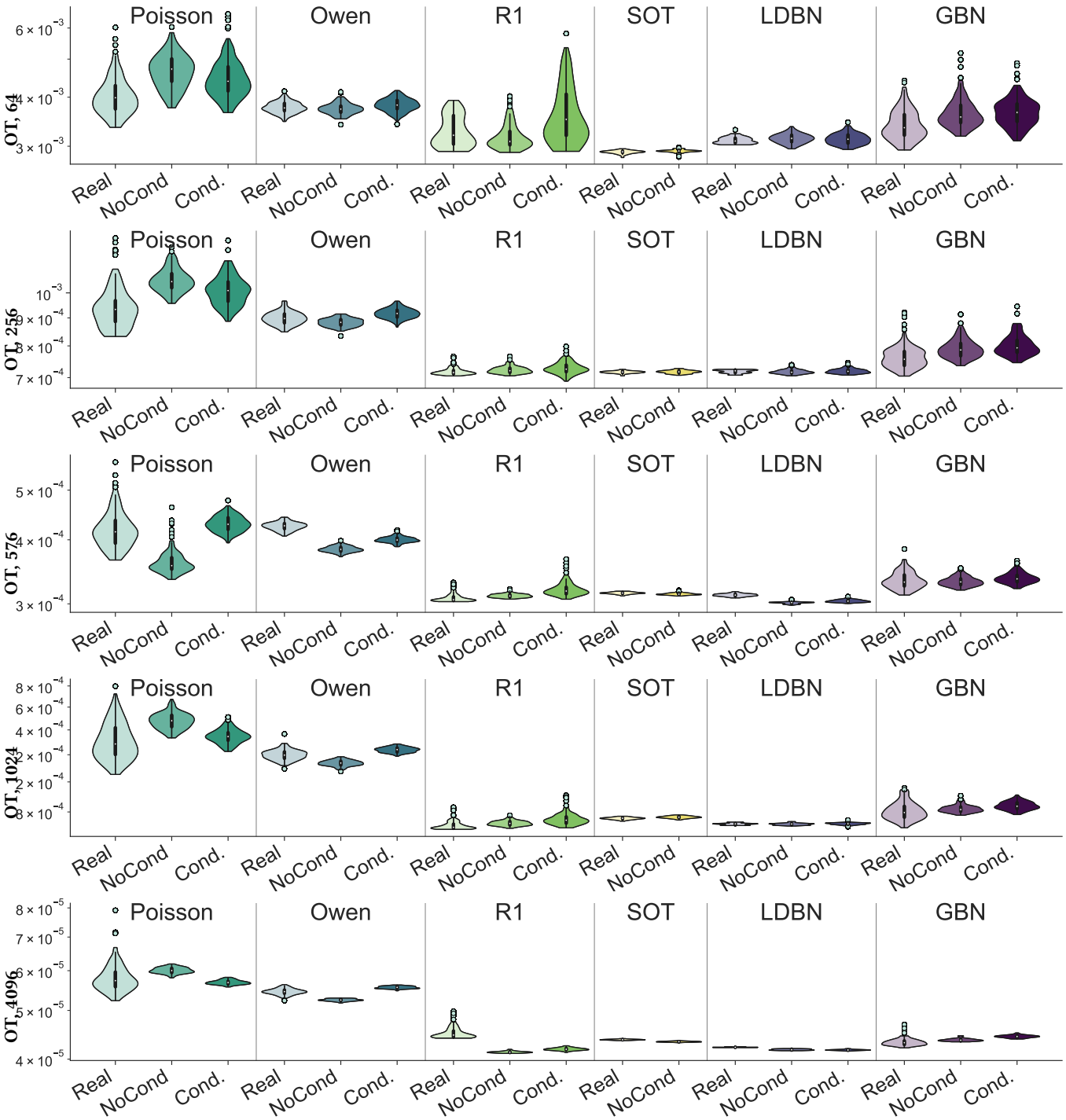


**Figure 3: Evaluation of the class conditioned model - optimal transport metric.**

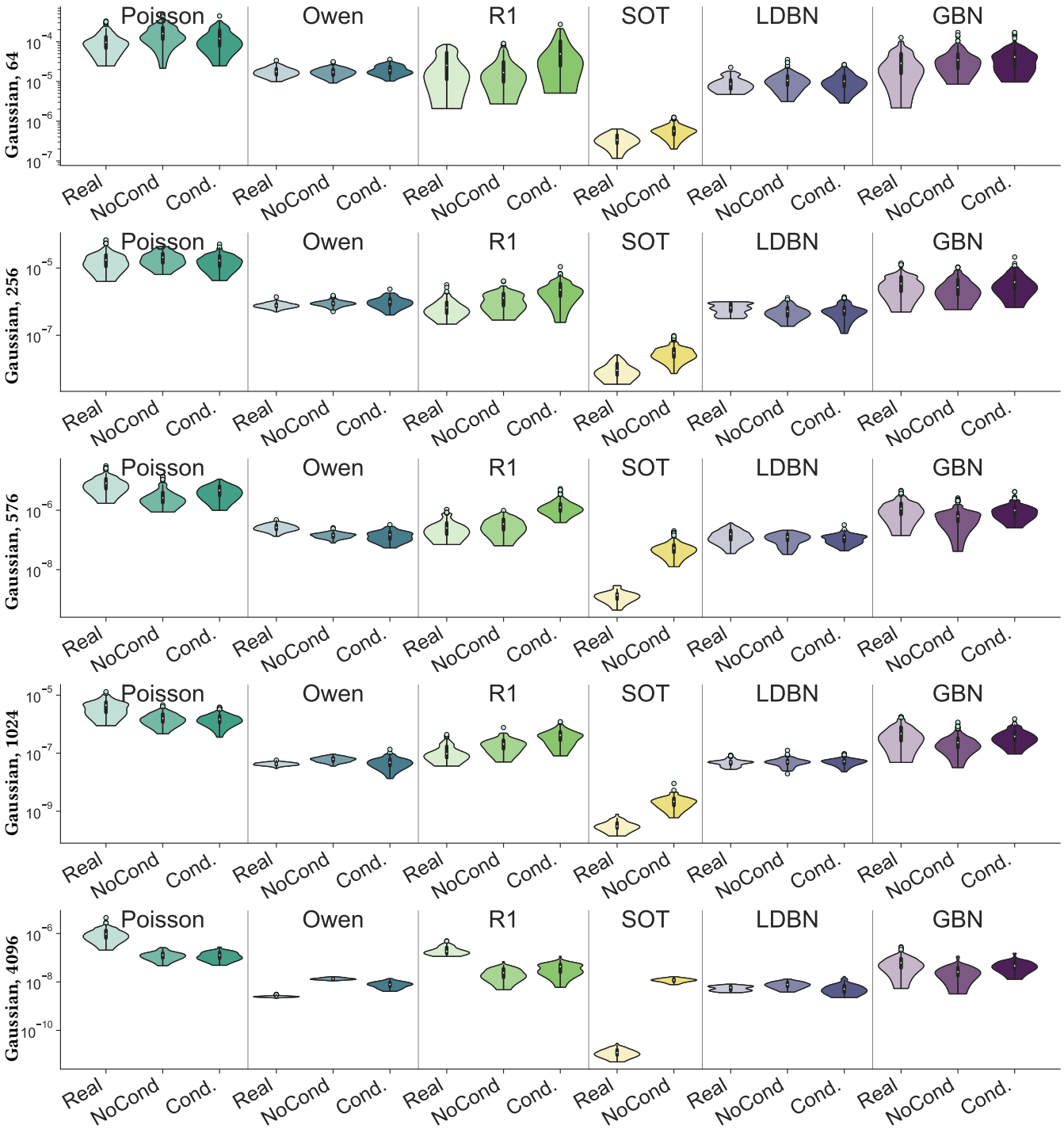


**Figure 4: Evaluation of the class conditioned model - integration error on Gaussian integrands.**

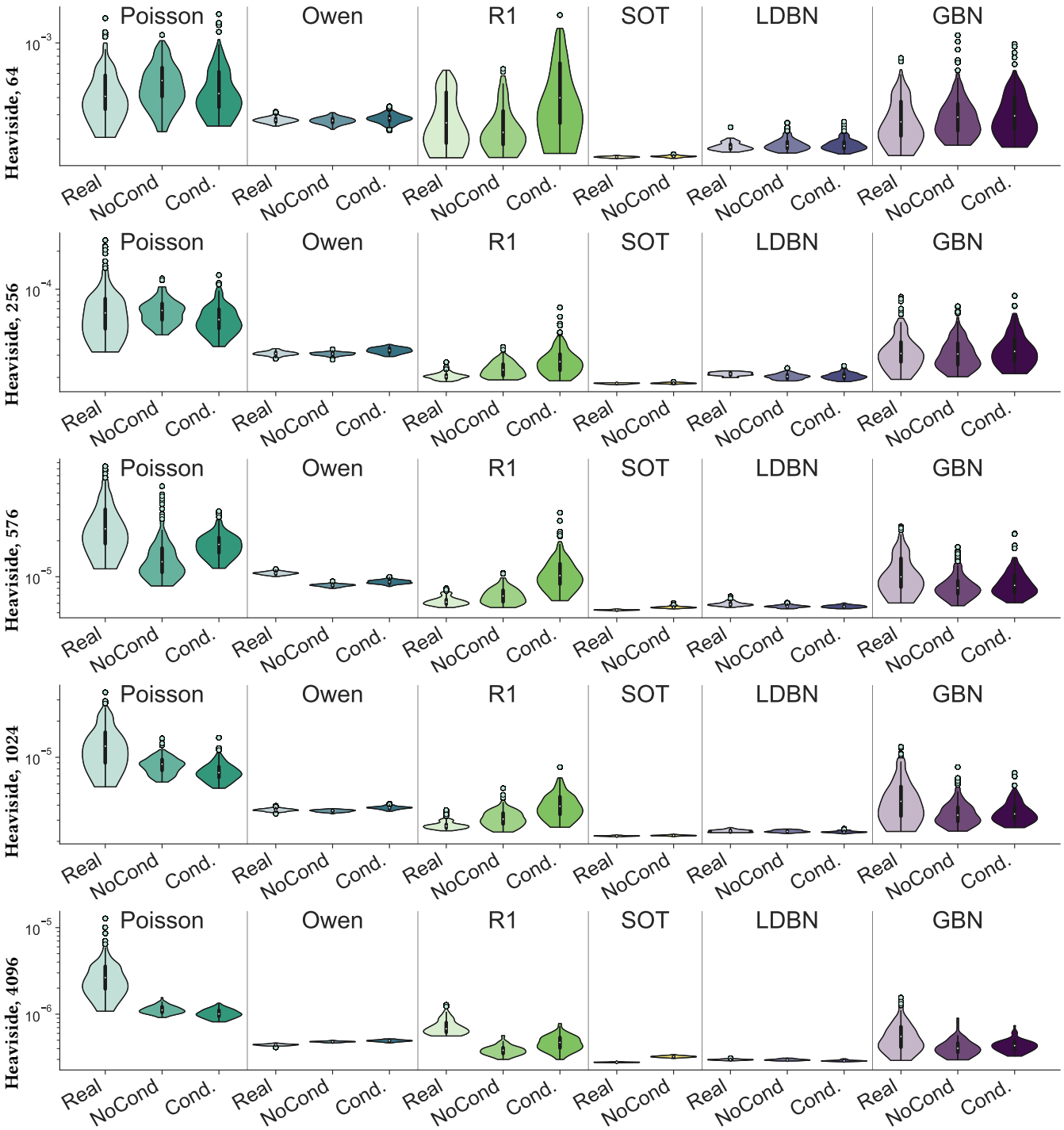


**Figure 5: Evaluation of the class conditioned model - integration error on Heaviside integrands.**

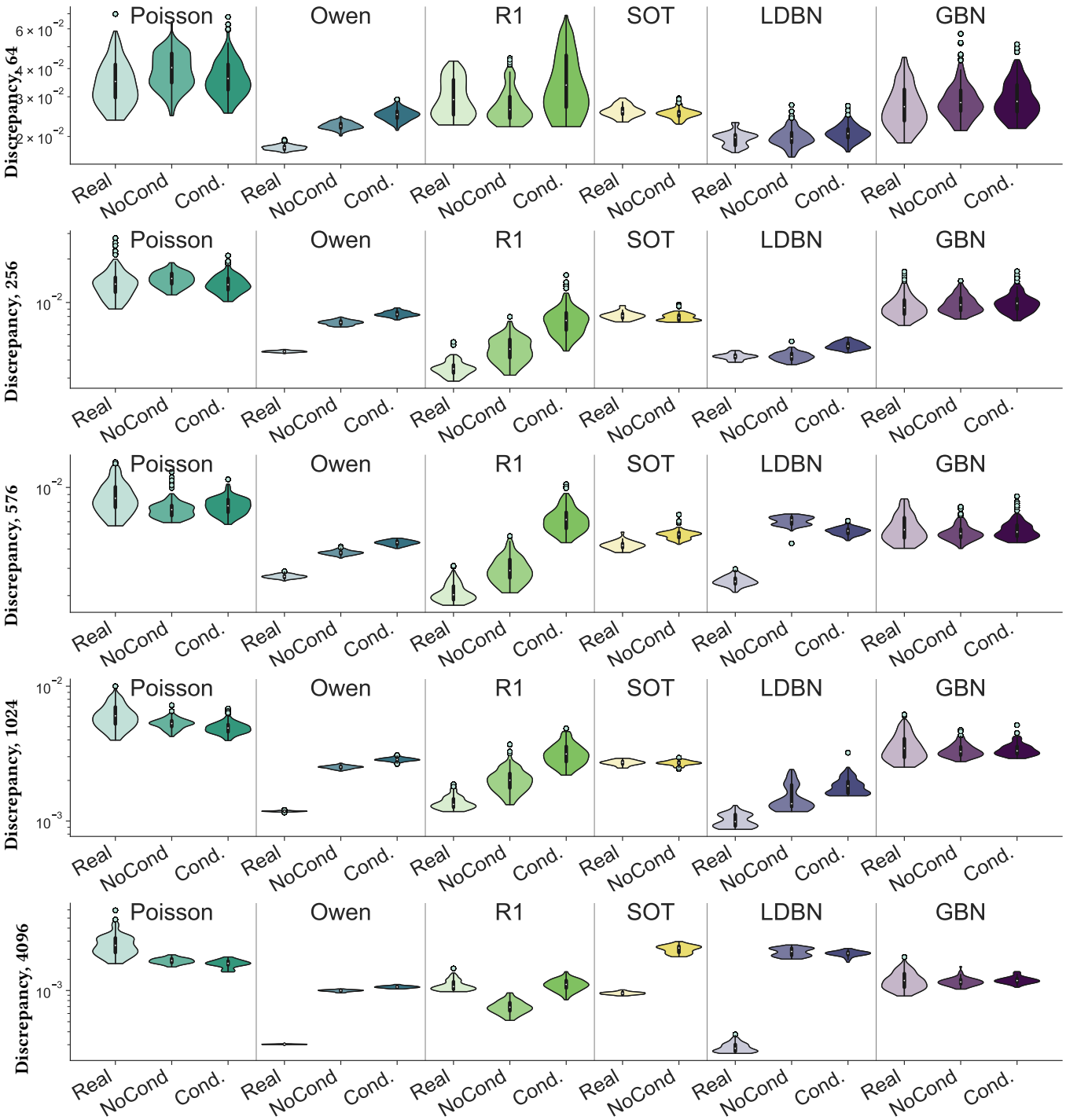


**Figure 6: Evaluation of the class conditioned model - generalized L2 discrepancy.**

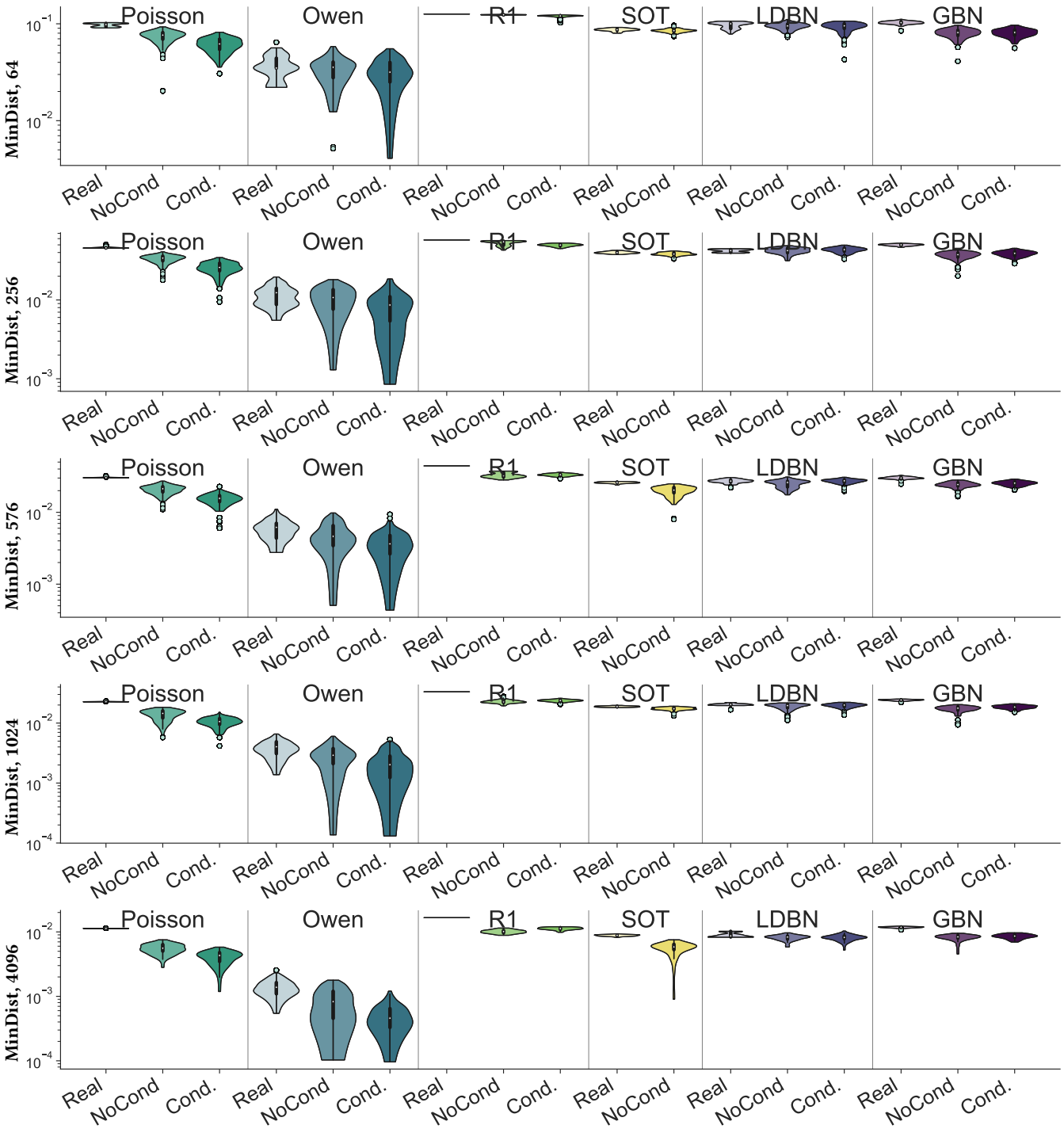


**Figure 7: Evaluation of the class conditioned model - minimum pairwise distance.**

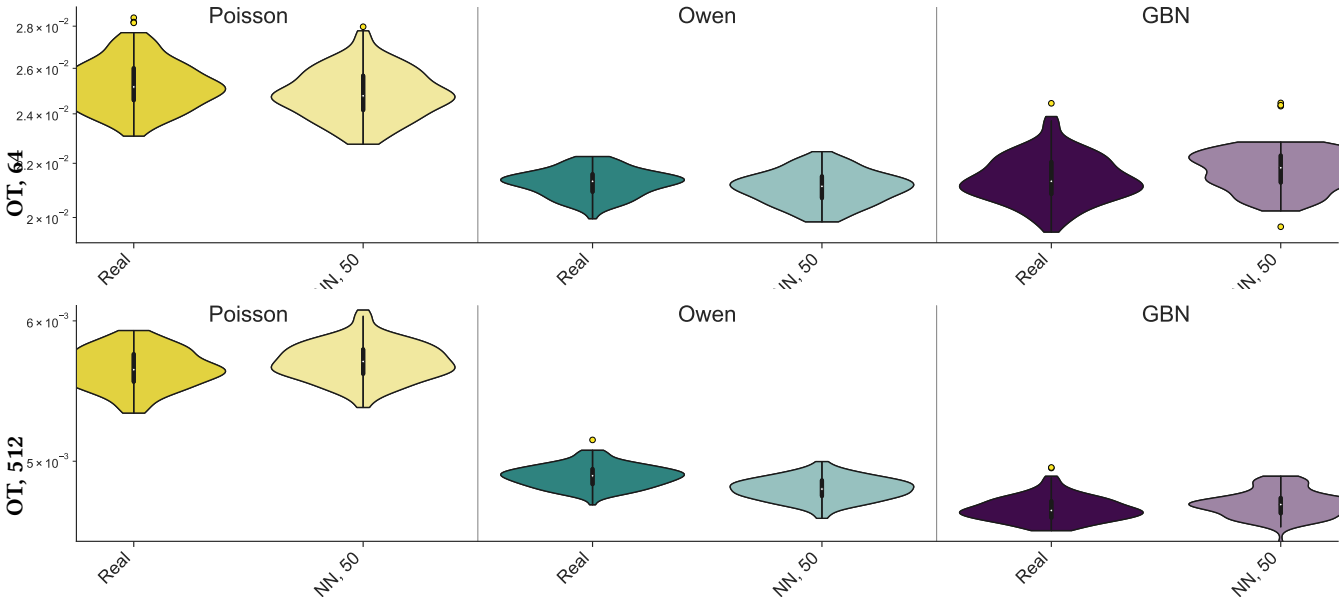


**Figure 8: 3D synthesis results - optimal transport metric.**

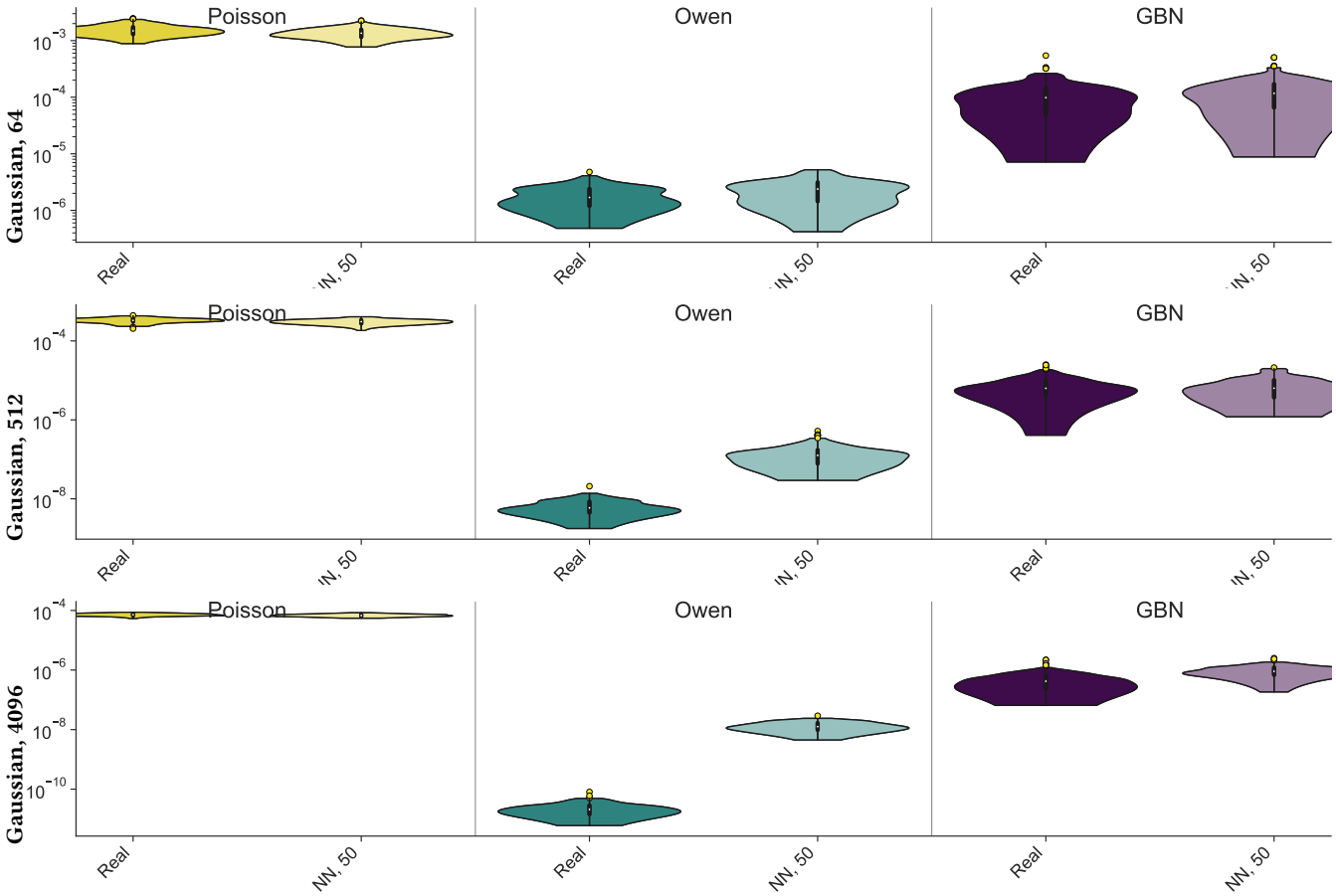


**Figure 9: 3D synthesis results - integration error on Gaussian integrands.**

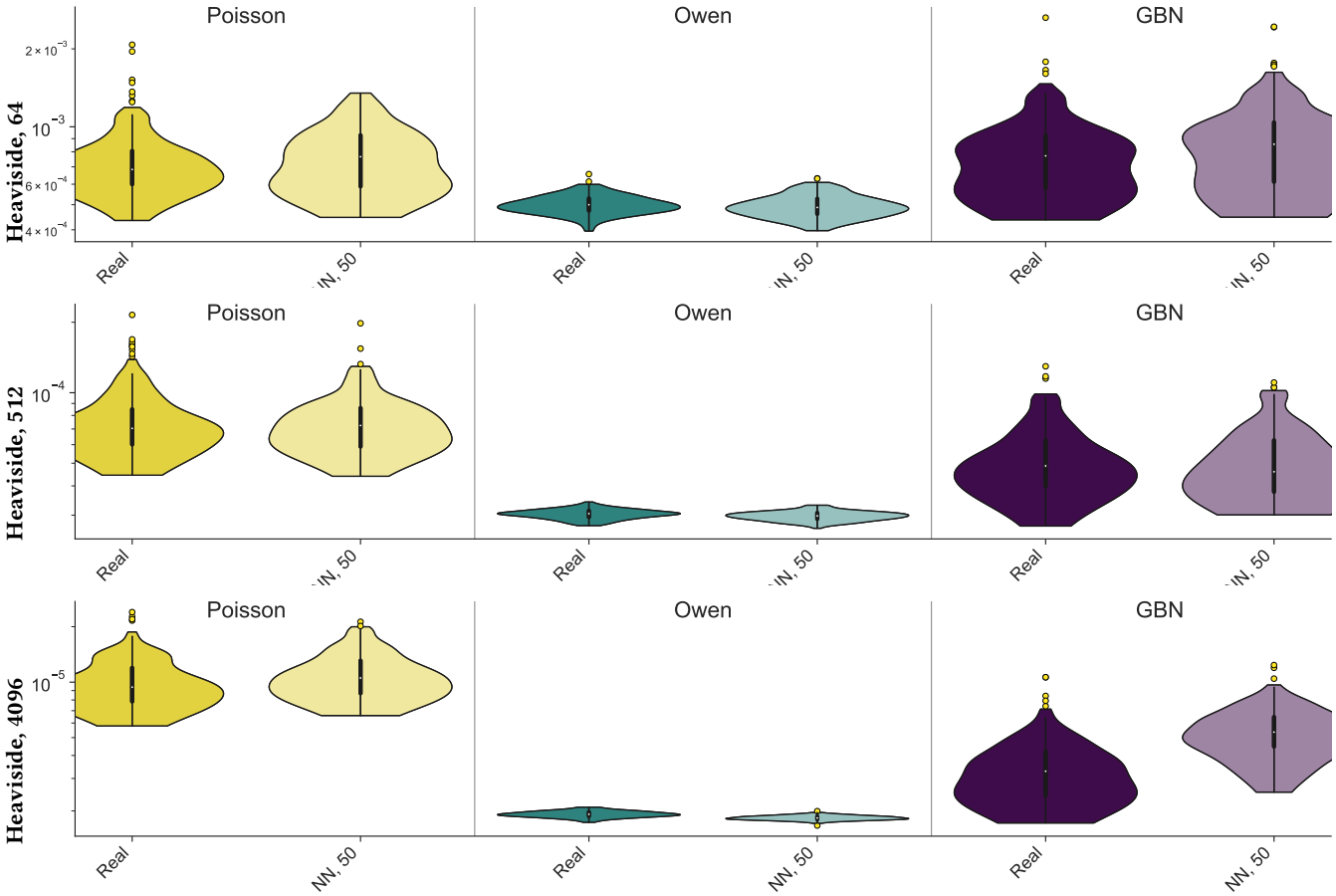


**Figure 10: 3D synthesis results - integration error on Heaviside integrands.**

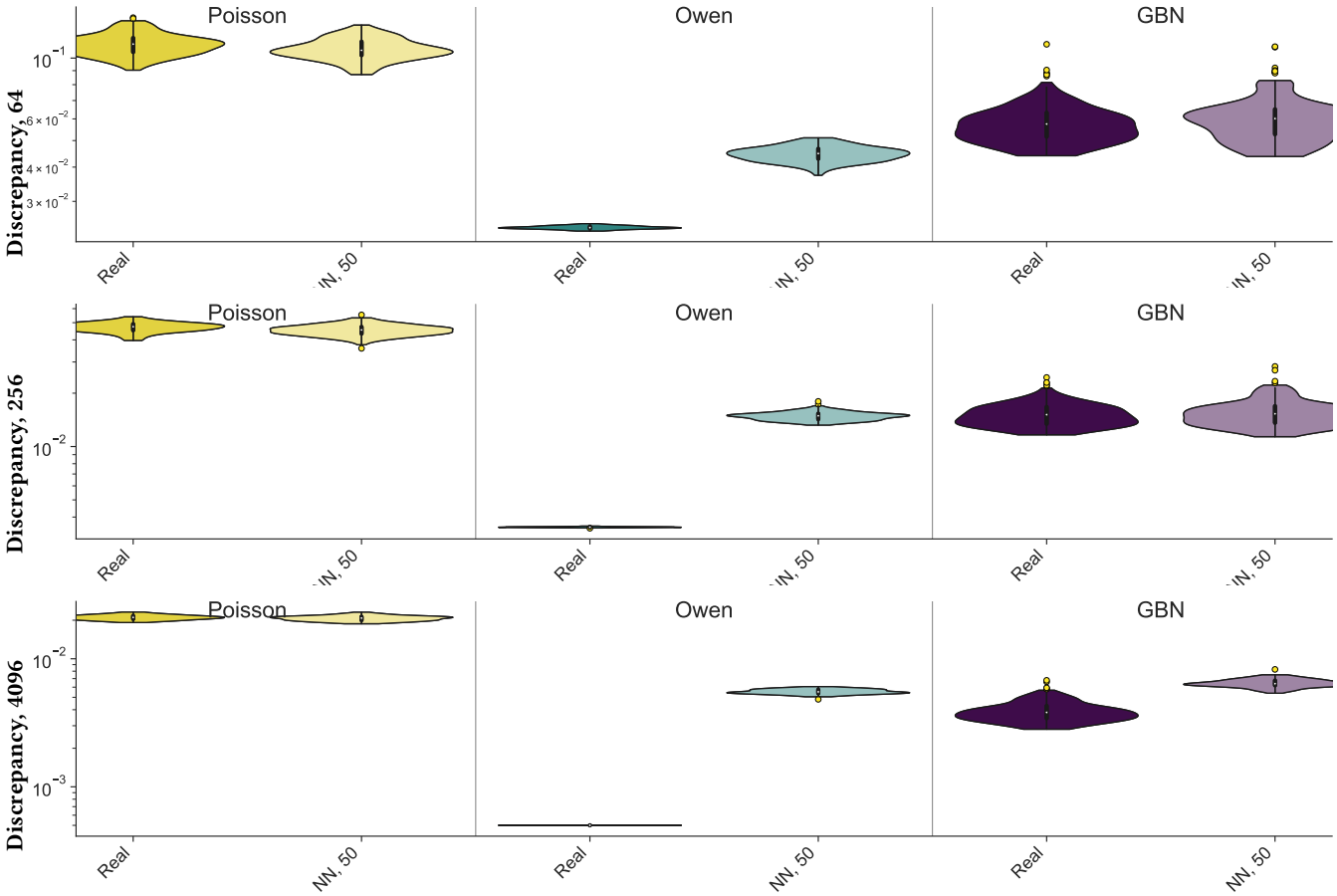


**Figure 11: 3D synthesis results - generalized L2 discrepancy.**

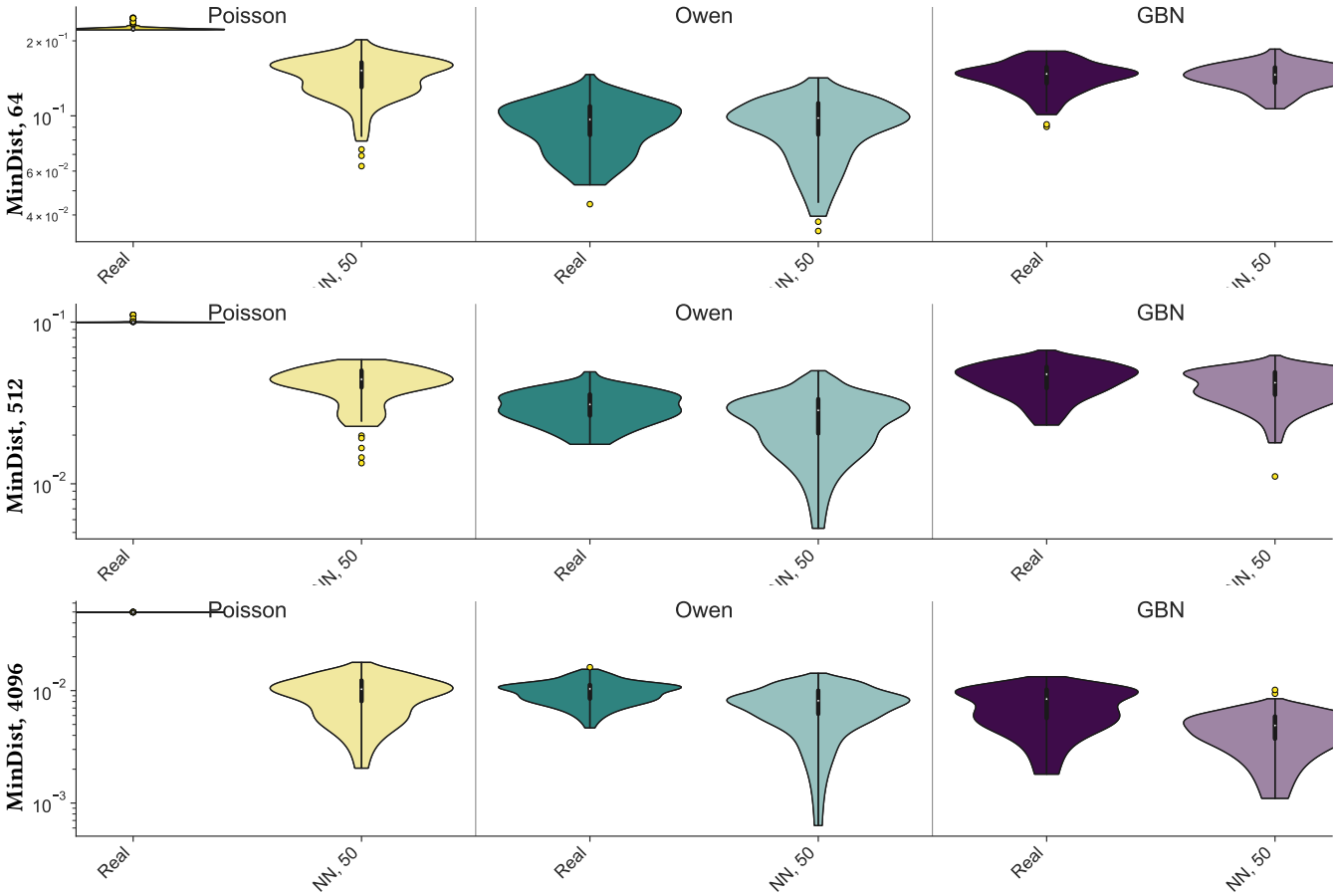


**Figure 12: 3D synthesis results - minimum pairwise distance.**

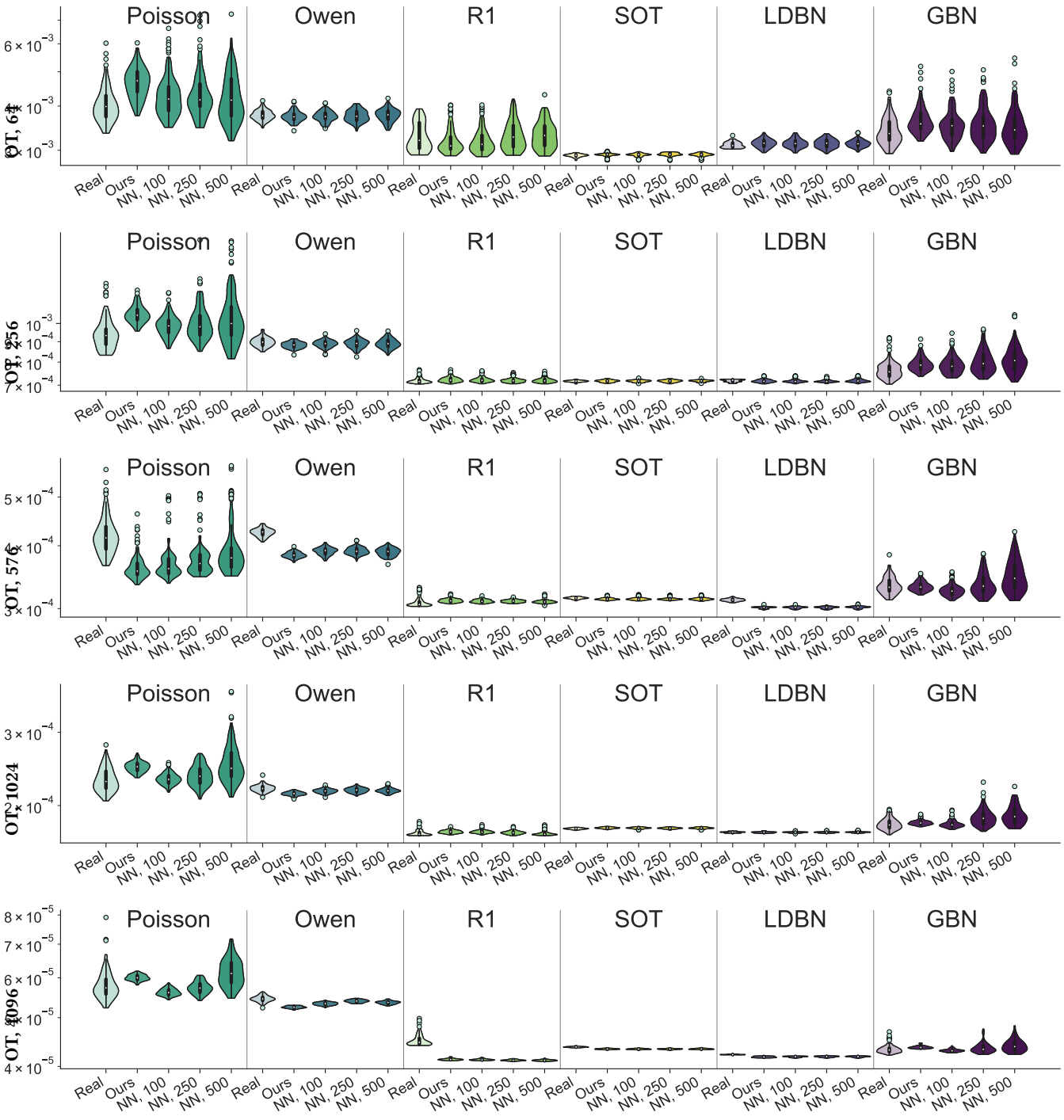


**Figure 13: Effect of reducing the number of diffusion steps at inference - optimal transport metric.**

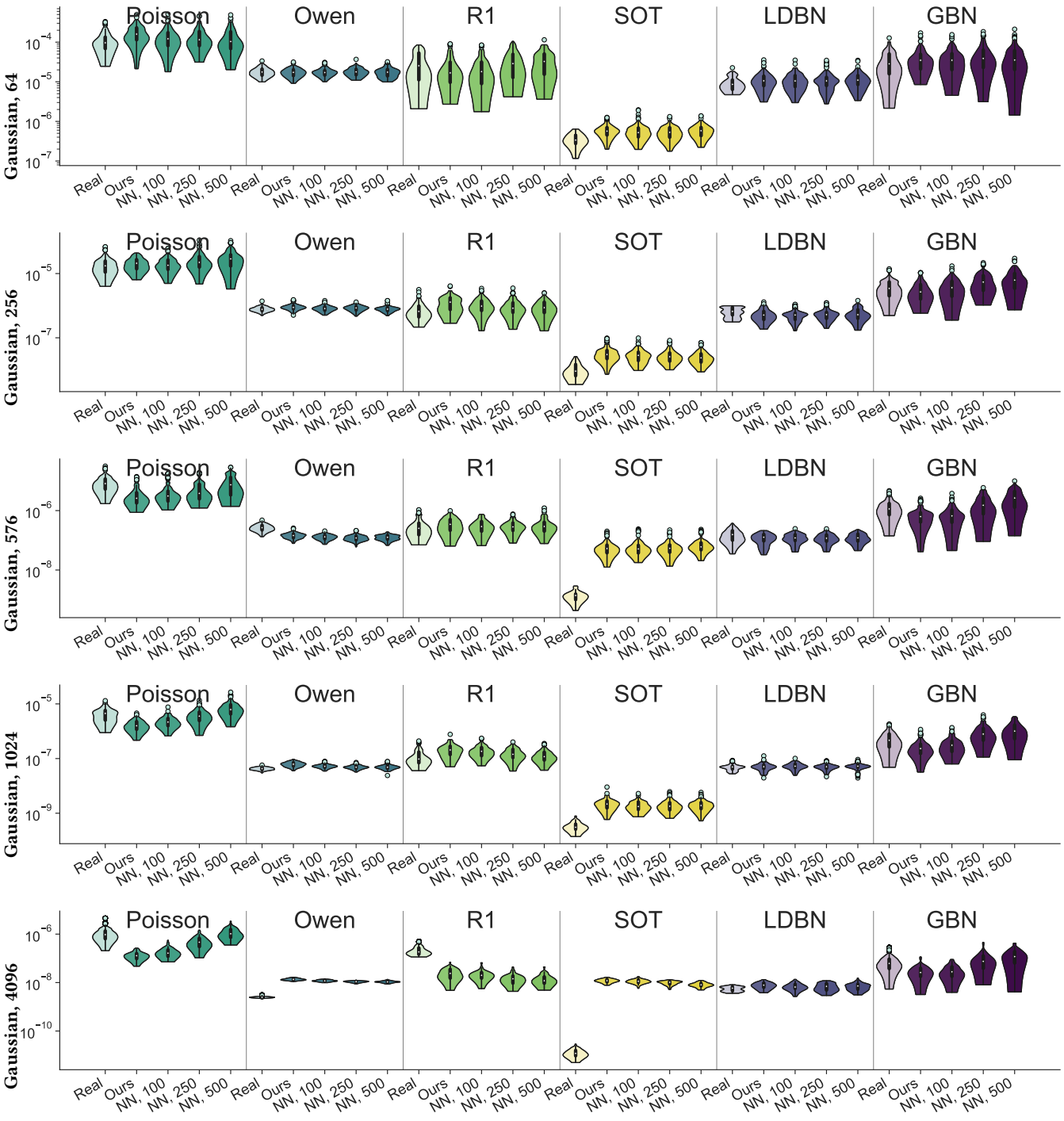


**Figure 14: Effect of reducing the number of diffusion steps at inference - integration error on Gaussian integrands.**

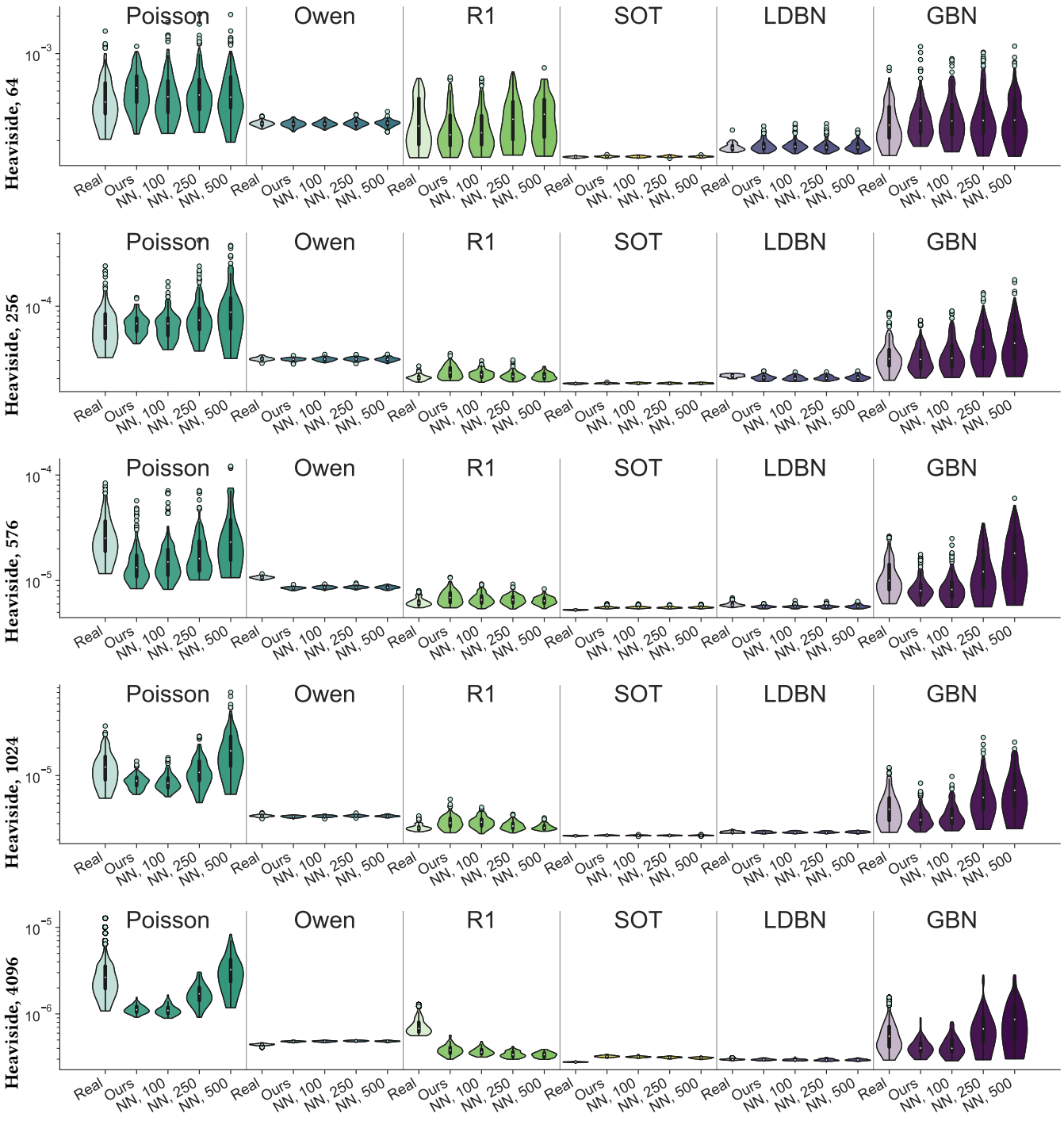


**Figure 15: Effect of reducing the number of diffusion steps at inference - integration error on Heaviside integrands.**

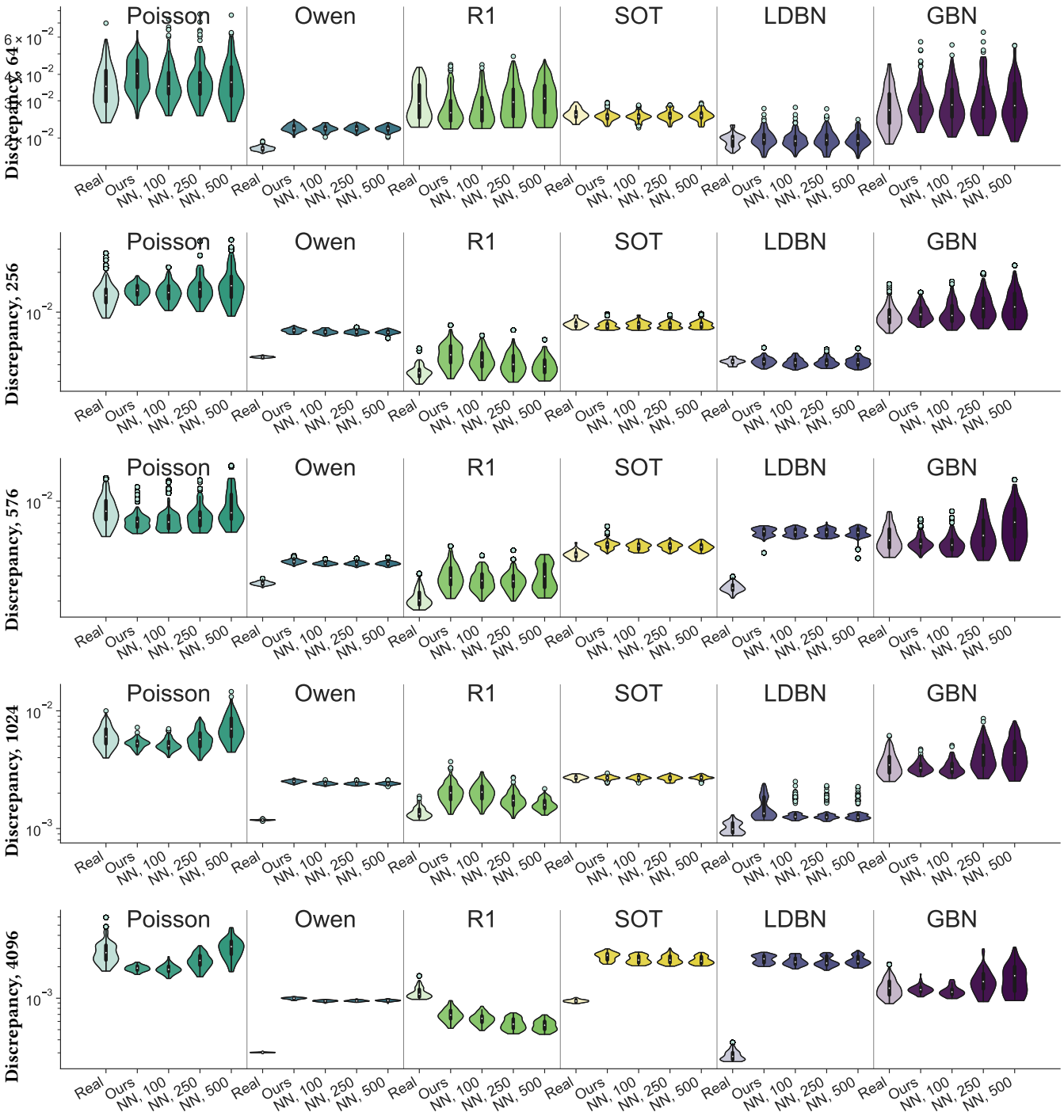


**Figure 16: Effect of reducing the number of diffusion steps at inference - generalized L2 discrepancy.**

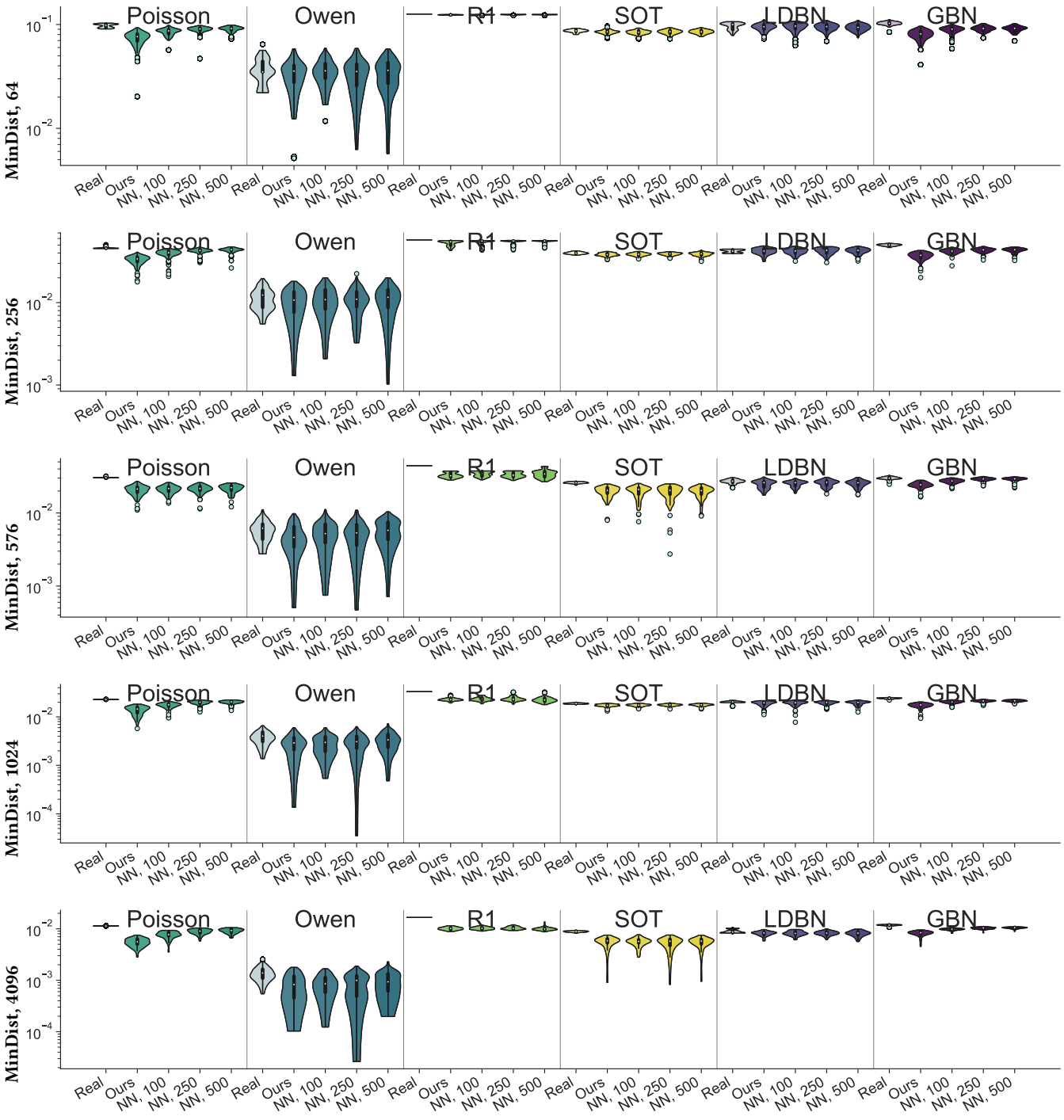


**Figure 17: Effect of reducing the number of diffusion steps at inference - minimum pairwise distance test.**

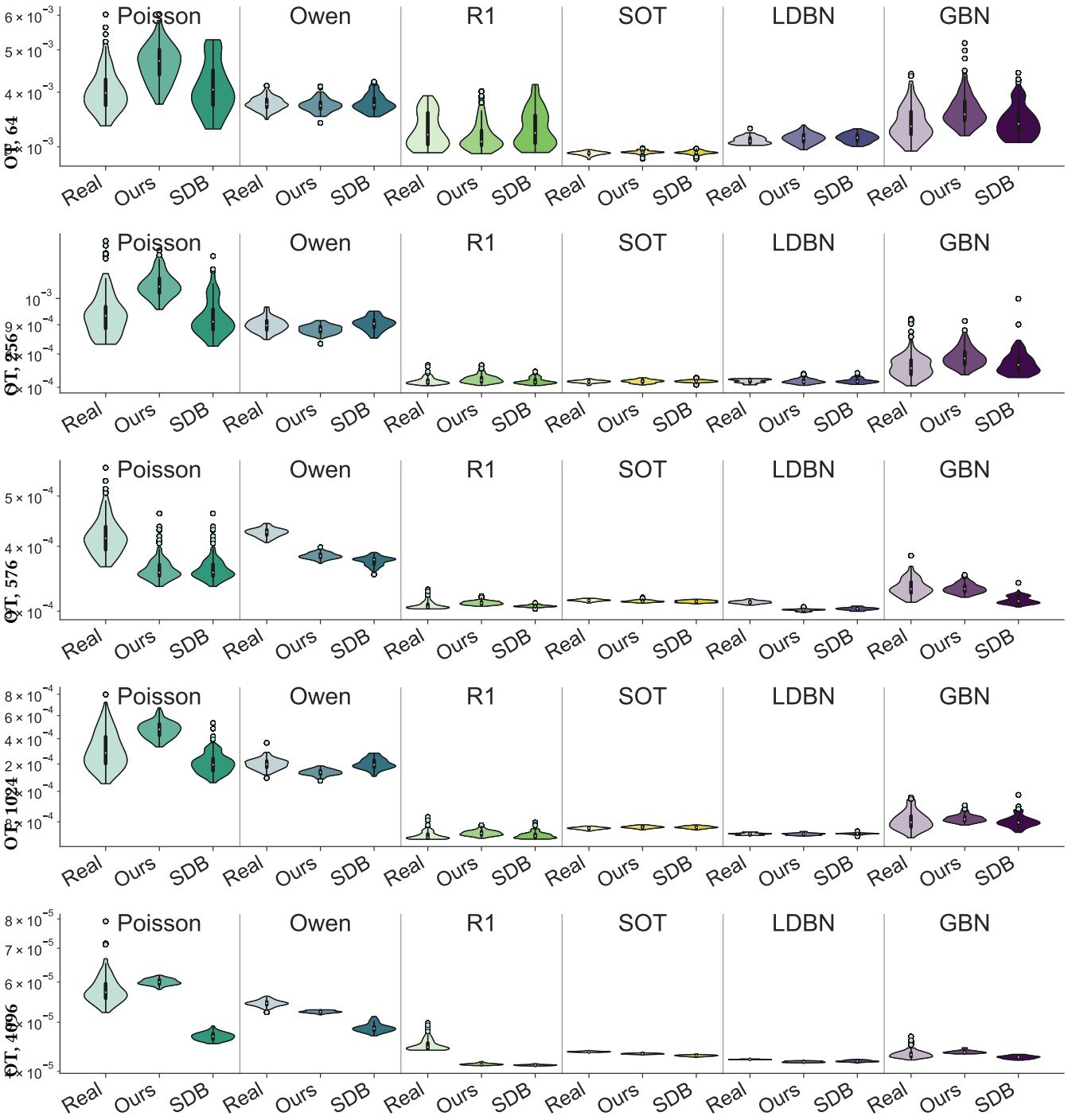


**Figure 18: Effect of the database size: optimal transport metric.**

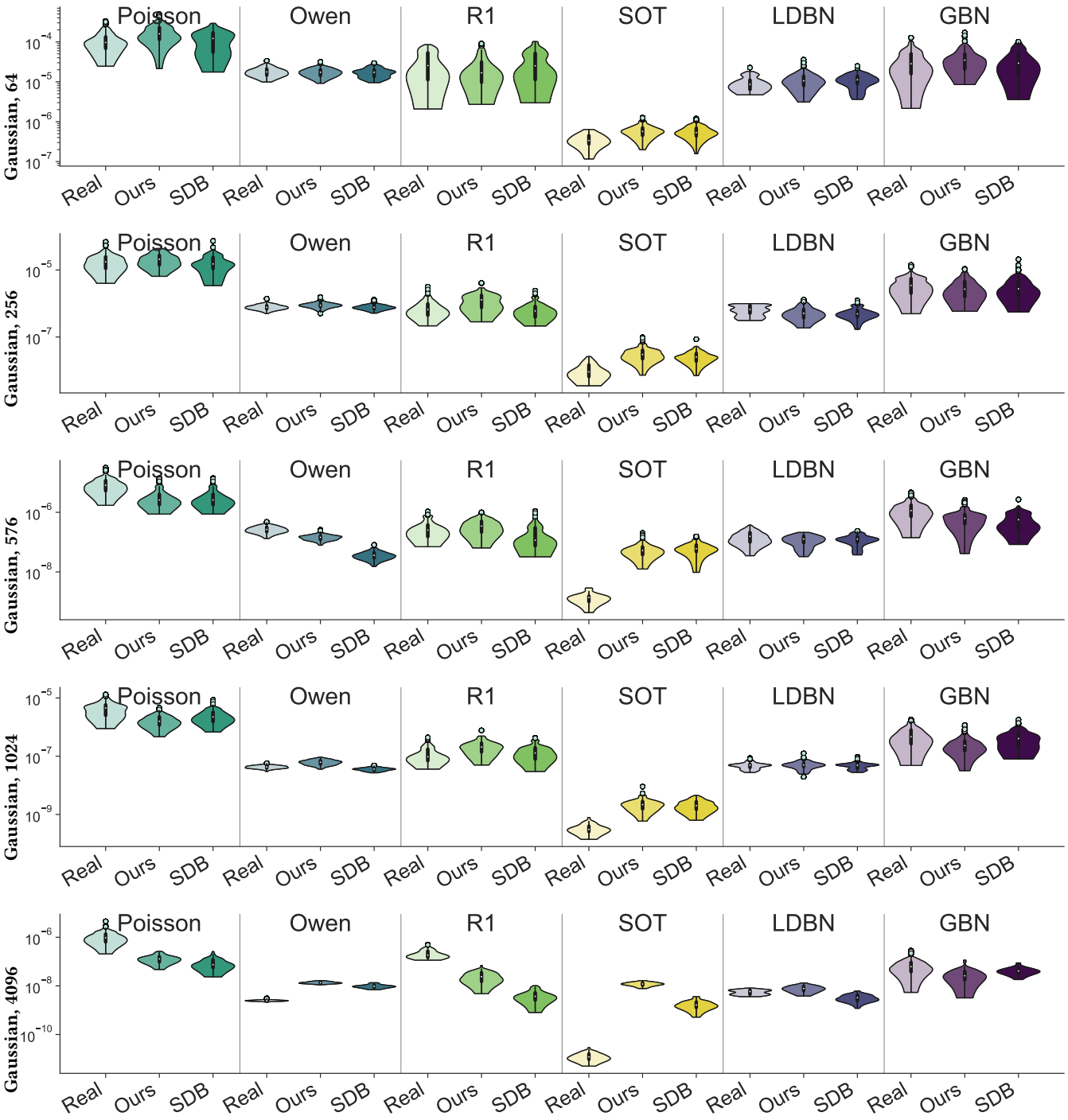


**Figure 19: Effect of the database size: integration error on Gaussian integrands.**

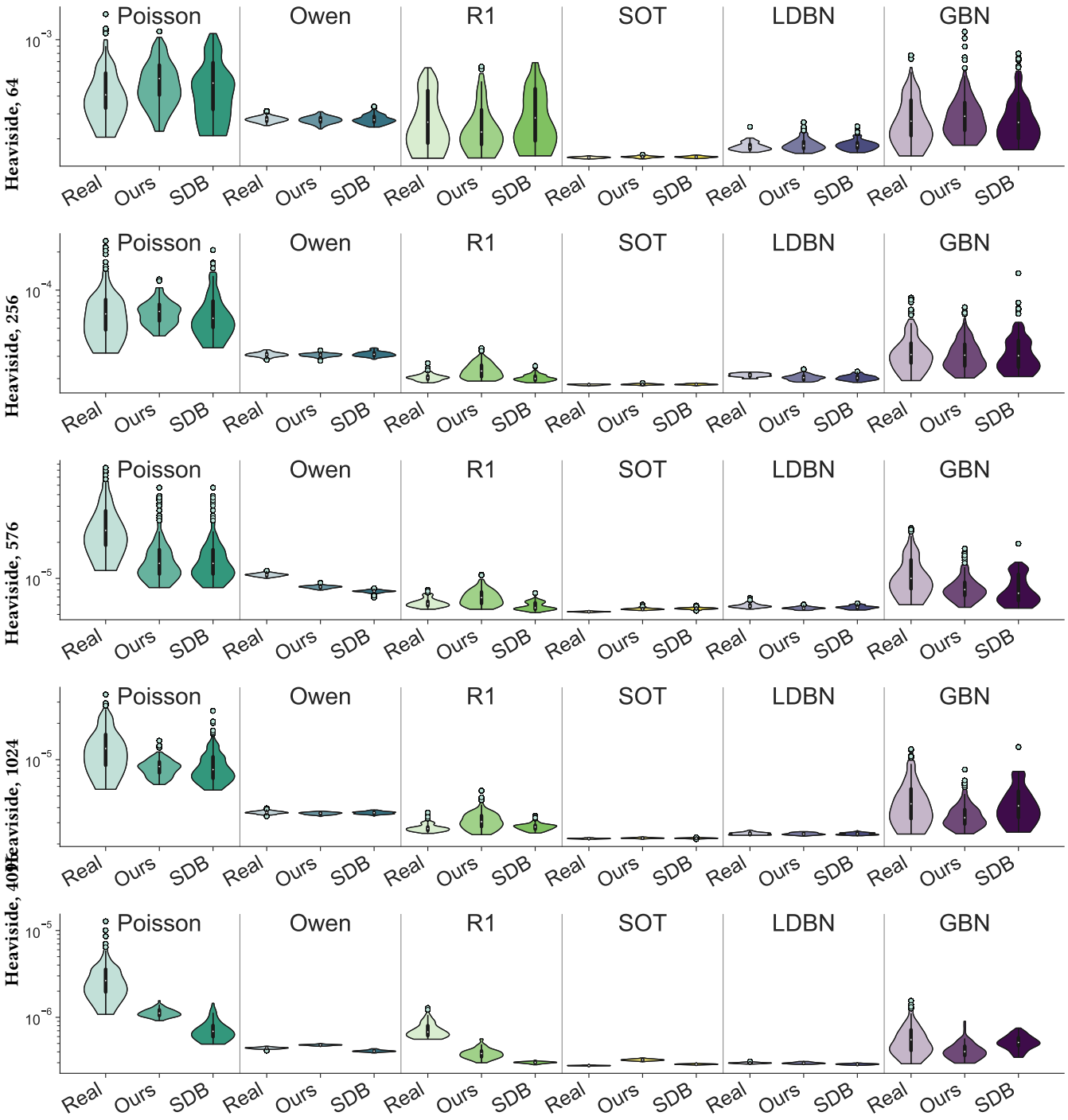


**Figure 20: Effect of the database size: integration error on Heaviside integrands.**

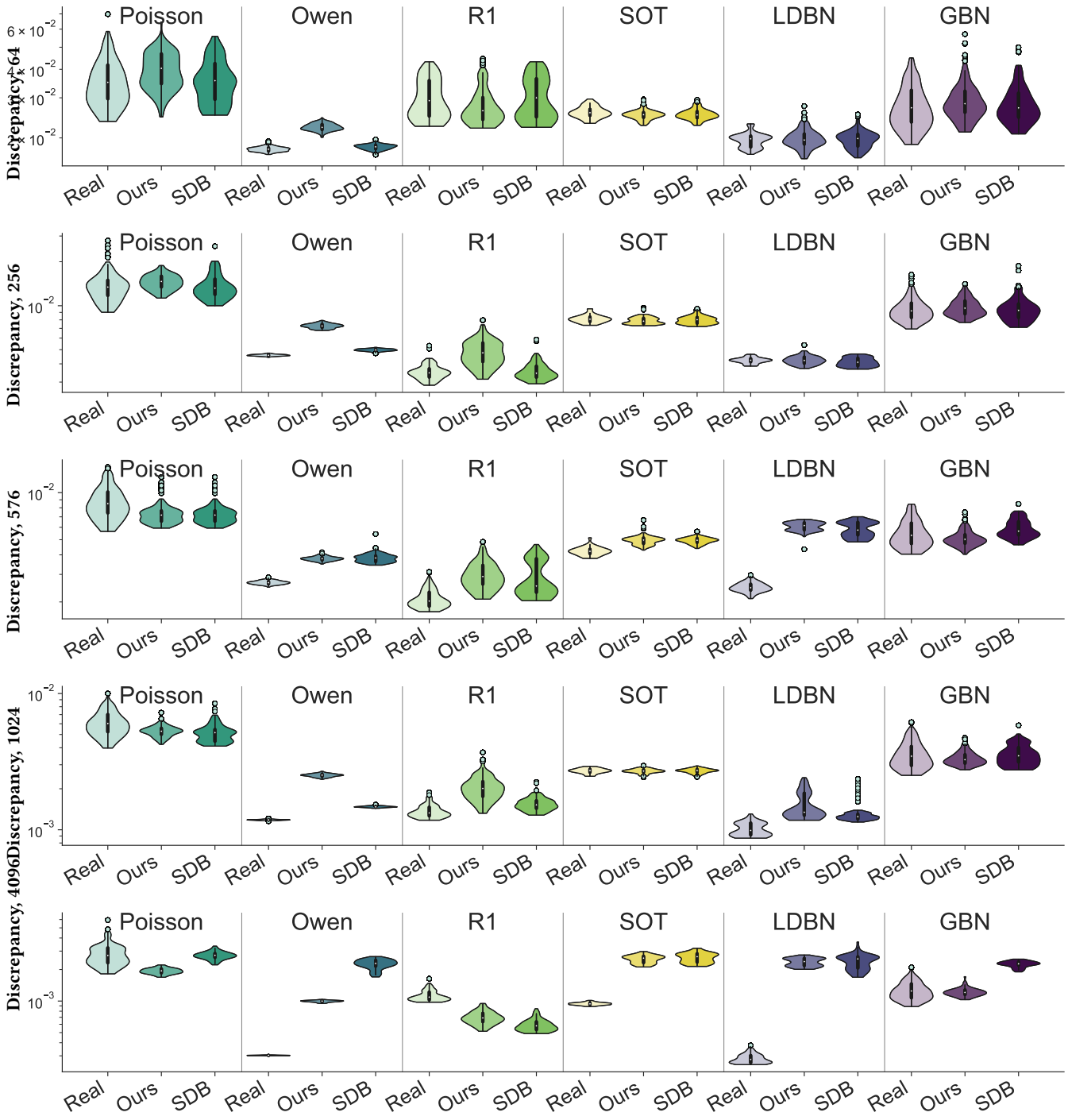


**Figure 21: Effect of the database size: generalized L2 discrepancy.**

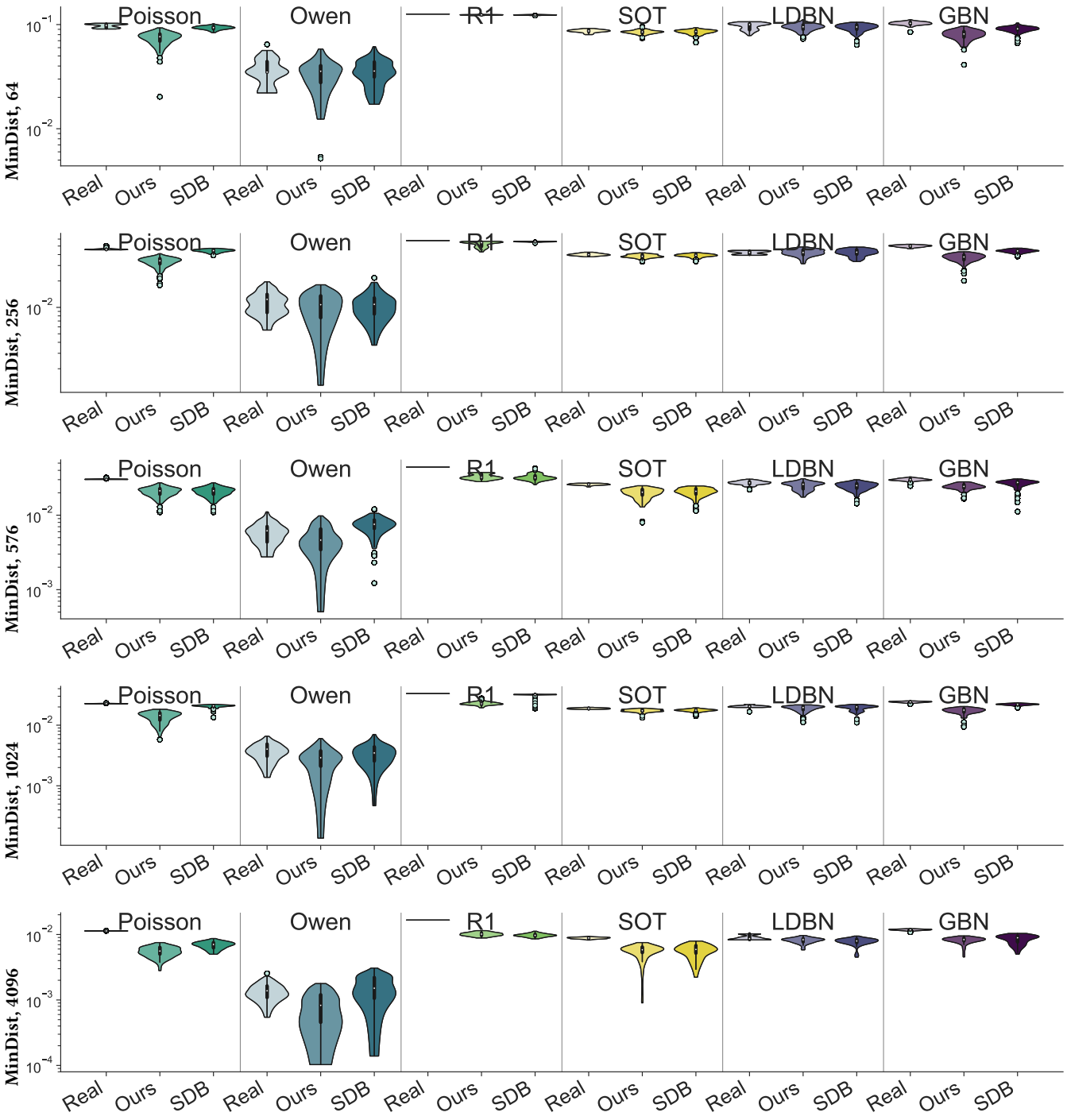


**Figure 22: Effect of the database size: minimum pairwise distance test.**